

**Six-quark decays of off-shell  $W^+W^-$  pairs  
via parton-level QCD  
in electron-positron annihilations**

S. Moretti\*

*Rutherford Appleton Laboratory,  
Chilton, Didcot, Oxon OX11 0QX, UK.*

**Abstract**

We study the decays into six quarks of off-shell pairs of  $W^\pm$  bosons produced in electron-positron annihilations, through the  $\mathcal{O}(\alpha_s^2)$  order in the strong coupling constant. We give explicit helicity amplitude formulae. We present numerical results in the context of phenomenological analyses of relevance at LEP2 and future Linear Colliders: such as  $M_W$  determinations, New Physics and Higgs searches.

---

\* E-mail: moretti@rl.ac.uk.

# 1 Introduction

Pairs of  $W^\pm$  bosons have copiously been produced at LEP2 and studied in great detail by the four experimental Collaborations over the past few years. In fact, one of the main goals of such collider is the determination of  $M_W$  with a target accuracy of 50 MeV or less. One of the detection strategies adopted to measure the  $W^\pm$  mass is the kinematic reconstruction of the  $W^\pm$  resonances through the momenta of their decay products, in the fully hadronic channel:  $W^+W^- \rightarrow$  jets. Although the event reconstruction is made hard in this decay mode by the large number of tracks in the detector and by the usual uncertainties related to measuring jet energies and directions, a task much less complicated in the case of semileptonic decays,  $W^+W^- \rightarrow 2$  jets  $\ell^\pm$  plus missing energy (with  $\ell = e, \mu, \tau$ ), and despite the existence of theoretical biases due to the relatively unknown ‘Bose-Einstein correlations’ [1] and ‘colour-rearrangement’ [2] effects, from which the semi-leptonic decays are immune, hadronic decays of  $W^+W^-$  pairs have been successfully exploited at LEP2. On the one hand, they yield the largest decay rate. On the other hand, the knowledge of all momenta in the final state helps tightening the  $W^\pm$  mass resolution.

The problem with the fully hadronic mode is twofold. Firstly, because two identical decays take place in the same event, one has the phenomenon of mis-pairing of jets. That is, even in the ideal case in which all hadronic tracks are correctly assigned to the parton from which they originate, one has to cope with the ambiguity that it is in practise impossible to uniquely assign any pair among the four reconstructed jets to the parent  $W^\pm$  on the sole basis of the event topology. Of all possible combinations of di-jet systems, only one is correct. Thus, an intrinsic background exists in  $W^+W^- \rightarrow 4$  jet events, in terms of simple combinatorics. Secondly, because of the large hadronic multiplicity, one also has the phenomenon of mis-assignment of tracks. This is induced by the procedure adopted in selecting jets. This is generally done by resorting to so-called jet clustering algorithms [3], wherein the number of tracks is reduced one at a time by combining the two most (in some sense) nearby ones. The joining procedure is stopped by means of a resolution parameter,  $y_{\text{cut}}$ , and the final ‘clusters’ are called jets. Here, the ambiguity stems from the fact that a track assigned to a cluster, the latter eventually identified as the parton originating from one of the  $W^\pm$ ’s, might have actually been produced in the fragmentation of another parton coming from the second  $W^\pm$  decay.

In both cases, the consequence is a distortion of the ‘line shape’ of the  $W^\pm$  resonance, which needs to be accurately quantified if one wants to achieve the foreseen precision in the  $W^\pm$  mass measurement. In order to estimate these effects, one can resort to phenomenological Monte Carlo (MC) programs (e.g., HERWIG [4], JETSET/PYTHIA [5] and ARIADNE [6]). These represent a valuable instrument in this respect, as they are able to describe the full event, from the initial hard scattering down to the hadron level. On the other hand, Matrix Element (ME) models are acknowledged to describe the large angle distributions of the QCD (and QED) radiation better than the former (see, e.g., [7, 8]), which are in fact superior in the small angle dynamics. Whereas the above MC programs have been in use for long time, so that their features need not being recalled here, it might be useful to review at this stage the progress made in ME calculations of  $e^+e^- \rightarrow W^+W^- \rightarrow$  jets, as many of the achievements in this field are very recent.

For a start, it should be mentioned that the amplitude for  $e^+e^- \rightarrow W^+W^- \rightarrow q\bar{q}q'\bar{q}'$  is very trivial to derive, in fact, more of a textbook example (here and in the following,  $q, q'$  and  $q''$

refer to (anti)quarks produced in the  $W^\pm$ ,  $W^\mp$  and  $g$  splittings, respectively). It represents the lowest-order (LO) contribution to the  $W^+W^- \rightarrow 4$  jet hadronic signal. Higher-order (HO) effects are those involving gluon emission: for example, the real one (i.e., a tree-level contribution) in  $e^+e^- \rightarrow W^+W^- \rightarrow q\bar{q}q'\bar{q}'g$  and  $e^+e^- \rightarrow W^+W^- \rightarrow q\bar{q}q'\bar{q}'gg$  events, which have been calculated in Refs. [9] and [10], respectively. One-loop QCD corrections to  $e^+e^- \rightarrow W^+W^- \rightarrow q\bar{q}q'\bar{q}'$  are also known to date [11], and they have been combined with the LO emission of Ref. [9] into the complete  $\mathcal{O}(\alpha_s)$  result [11].

It is purpose of this paper to study the reaction  $e^+e^- \rightarrow W^+W^- \rightarrow q\bar{q}q'\bar{q}'q''\bar{q}''$  at tree-level, through the order  $\mathcal{O}(\alpha_{em}^4\alpha_s^2)$ . Earlier accounts of this process, with emphasis on it being a background to top-antitop production and decay at a future Linear Collider (LC), were given in Ref. [12]. The complete set of Feynman diagrams needed to perform such a calculation can be found in Fig. 1. The plan of the paper is as follows. In the next Section we highlight the phenomenological impact at LEP2 and a LC of six-quark production via  $W^+W^-$  decays. In Sect. 3 we describe our method of computation using tree-level perturbative QCD. In Sect. 4 we present our results whereas Sect. 5 contains our conclusions.

## 2 Phenomenology of six-quark decays of $W^+W^-$ pairs

In our opinion, there are a few good reasons to tackle the calculation of the process  $e^+e^- \rightarrow W^+W^- \rightarrow q\bar{q}q'\bar{q}'q''\bar{q}''$ .

As for  $M_W$  determinations, one should note the following.

1. The availability of all HO corrections to the leading four-parton decay of  $W^\pm$  pairs is essential, both at tree and loop level, for the following reasons. On the one hand, from the point of view of perturbative calculations, it is evident that the 4-jet rate is constituted not only of the fraction of 4-parton events in which all partons are resolved (i.e., their separation is above the cut-off  $y_{\text{cut}}$ ), but also by the  $(4 + m)$  parton configurations (with  $m \geq 1$ ) in which  $m$  partons remain unresolved. On the other hand, because of the way an experimental 4-jet sample of  $W^+W^-$  events is normally selected (see, e.g., [13]), also the  $(4 + m)$  parton contributions with  $m$  jets resolved are relevant, as they naturally enter the candidate experimental sample of hadronic decays of  $W^+W^-$  pairs. In fact, in order to maximise the event rate of the signal, one usually requires to reconstruct *at least* four jets, all with separation above a minimum  $y_{\text{cut}}$ . Only eventually these jets are forced into exactly four, by merging together those which are ‘closer’. In this respect, one subtlety should be noted concerning  $W^+W^- \rightarrow 6$  quark events. The diagrams shown in Fig. 1 implicitly assume that the flavour of the quarks produced in the gluon splitting, labelled by 7 and 8, is different from that of any of the fermions generated by the  $W^\pm$  decays, indicated by 3, 4, 5 and 6. In fact, in case one or two quarks (or antiquarks) are identical, the numbers of diagrams doubles or quadruples, respectively, the new graphs being obtained from the old ones by exchanging one or two identical fermion legs, in all possible ways (a minus sign factorises too, for any of these exchanges). This follows from the fact that the flavour of a quark and its origin (i.e., whether it comes from a  $W^\pm$  or a  $g$ ) are indistinguishable in the experimental hadronic sample. From the point of view of  $W^\pm$  mass studies, it is evident that this is source of two types of systematic effects. Firstly,

the total rate of  $W^+W^- \rightarrow 6$  quark decays naively obtained by summing over five flavours in the  $g^* \rightarrow q''\bar{q}''$  splitting (the approach used in parton shower models) could be mis-estimated. Secondly, additional distortion effects to the line-shape of the  $W^\pm$  resonance could occur. In the spirit of Refs. [1, 2], the reader should not object to calling such effects ‘flavour-rearrangement’ or ‘Fermi-Dirac correlations’.

We further focus on possible New Physics and Higgs boson searches.

2. The very fact that one of the two  $W^\pm$ 's has a chance to decay into four jets reproduces at LEP2 and a LC a dynamics similar to that analysed in several instances at LEP1, when studies of  $\gamma^*, Z \rightarrow 4$  jet decays were performed<sup>1</sup>, in view of the possible existence of New Physics contributions due light gluinos  $\tilde{g}$  of the MSSM [14]. The evidence of such effects at LEP1 was mainly searched for in the context of the measurement of the three fundamental colour factors of QCD:  $C_A$ ,  $C_F$  (the Casimir operators of the fundamental and adjoint representations of the gauge group  $SU(N_C)$ , respectively) and  $T_F$  (the normalisation of the generators of the fundamental representation). In fact, under the assumption that  $SU(N_C \equiv 3)$  is indeed the gauge group of QCD, with  $N_C$  the number of colours, a measurement of these parameters (in particular of  $T_R = N_F T_F$ ) can be converted into a constraint on the number of coloured fermions active at the energy scale at which the decay takes place. For example,  $N_F$  would be increased (by approximately 3) from its SM value at LEP energies (i.e.,  $N_F = 5$ ) by the additional presence of gluinos produced via a  $g \rightarrow \tilde{g}\tilde{g}$  splitting [15]. In ordinary QCD, one gets  $C_A = 3$  and  $C_F = 4/3$  (also,  $T_F = 1/2$ ). Since the results of these analyses have not excluded the possible existence of Supersymmetric (SUSY) events in LEP1 data in the form of very light gluinos, with mass below 1–1.5 GeV [7, 16], we consider whether contributions of  $e^+e^- \rightarrow W^+W^- \rightarrow q\bar{q}q'\bar{q}'\tilde{g}\tilde{g}$  events possibly entering the six-jet sample produced at LEP2 and a LC can at all be disentangled. (Notice that the above mass region has escaped also the LEP1 limits imposed through the running of  $\alpha_s$ , at the three-loop perturbative level [17], in hadronic decays of heavy particles [18] (e.g.,  $Z$  and  $\tau$ ), as well as those obtained from other experiments (KTeV, NA48, E761) searching for decays of gluino bound states<sup>2</sup>, see [21].) The much reduced  $W^+W^-$  cross section at LEP2 and a LC, as compared to the  $Z$  one at LEP1, clearly disfavors such a possibility. In contrast, it would be intriguing to consider a selection strategy similar to that advocated in Ref. [22], based on the detection of a secondary vertex possibly due to a gluino decay with lifetime between, say,  $10^{-12}$  (the typical scale of  $b$  and  $c$  quarks) and

---

<sup>1</sup>Not quite, it could well be argued, given that in  $W^+W^- \rightarrow 6$  quark decays one has to first isolate a subset of four jets which come from the same  $W^\pm$  decay, out of the original six, and since such an operation is in principle affected by the same mis-assignment problems already described. In practise, we will show that is rather easy to select such a subject, the latter preserving the typical angular properties of gauge bosons and fermions exploited in the experimental fits (see discussion later on).

<sup>2</sup>Some possible, Supergravity (SUGRA) inspired decay modes are [19]:  $R^0 \rightarrow \pi^+\pi^-\tilde{\gamma}$  and  $R_p \rightarrow S^0\pi^+$ , where  $R^0$  is the so-called glueballino bound state  $R^0 \equiv (g\tilde{g})$  and the ‘photino’  $\tilde{\gamma}$  is the lightest SUSY particle (LSP), whereas  $R_p \equiv (uud\tilde{g})$  and  $S^0 \equiv (uds\tilde{g})$ , with  $S^0 \rightarrow R^0\Lambda$ . The mass(lifetime) of the  $R^0$  is set by the theory to be in the range 1.4 – 2.2 GeV( $10^{-5} - 10^{-10}$  sec) whereas that of the  $R_p$  is 1.6 – 3.1 GeV( $2 \cdot 10^{-10} - 2 \cdot 10^{-11}$  sec). For alternative decay modes, in the Gauge Mediated SUSY breaking scenario, which have recently been proposed and not yet exploited experimentally, see Ref. [20].

$10^{-9}$  (the coverage of the LEP detectors) sec. Besides, the fact that a  $W^\pm$  cannot decay directly into  $b$  quarks (apart from Cabibbo-Kobayashi-Maskawa suppressed channels, that we neglect here) implies that at LEP2 and a LC the overwhelming background from ordinary QCD due to  $e^+e^- \rightarrow W^+W^- \rightarrow q\bar{q}q'\bar{q}'gg$  events, with  $q^{(\prime)} \neq b$ , should effectively be removed by asking for just a single vertex tagging displaying a decay length comparable or longer than that induced by  $b$  quarks,  $d_b \approx 0.3$  mm. This way, the surviving six-jet sample would only be composed by  $e^+e^- \rightarrow W^+W^- \rightarrow q\bar{q}q'\bar{q}'b\bar{b}$  and  $e^+e^- \rightarrow W^+W^- \rightarrow q\bar{q}q'\bar{q}'\tilde{g}\tilde{g}$  events. These have comparable production rates, which is a most welcome result. After all, the smallness of the SUSY effect with respect to ordinary QCD dynamics was really the limiting factor of the experimental analyses performed at LEP1, given that even the very large next-to-leading-order (NLO) corrections to the four-jet sample leave the shape of the distributions used to fit  $C_A$ ,  $C_F$  and  $T_F$  practically unaltered [23]. For all the above reasons, we believe it then important looking into this aspect of six-jet phenomenology.

3. Finally, we consider the possibility that six-quark decays of  $W^+W^-$  pairs with a gluon splitting into  $b\bar{b}$  pairs, i.e.,  $e^+e^- \rightarrow W^+W^- \rightarrow q\bar{q}q'\bar{q}'b\bar{b}$  events, can act as a background to Higgs signals possibly produced at a LC. In the Standard Model (SM) one has the production mechanism  $e^+e^- \rightarrow \phi Z$ , whereas in the Minimal Supersymmetric Standard Model (MSSM) one can have two,  $e^+e^- \rightarrow \Phi Z$  and  $e^+e^- \rightarrow \Phi A$ , where  $\Phi = H, h$  represents any of the two scalar Higgs bosons of the SUSY theory and  $A$  is the pseudoscalar one. If one recalls that  $Z$  bosons decay into bottom quark pairs some 15% of the times and that the SM Higgs decay channel  $\phi \rightarrow W^+W^-$  is the one with largest branching ratio (BR) for  $M_\phi \gtrsim 140$  GeV, then it is evident that a very large part of the SM Higgs signal at a LC would appear through a six-jet signature, further considering that each  $W^\pm$  boson decays hadronically with a 70% BR. Similarly, in the MSSM<sup>3</sup>, the  $H \rightarrow W^+W^-$  (of the heavy scalar Higgs) decay rate can be very large on a big portion of the  $(M_A, \tan\beta)$  plane (especially for Higgs masses below the top-antitop decay threshold and at low  $\tan\beta$  [24]) and so is the case of the  $h \rightarrow W^+W^-$  (of the light scalar Higgs) one, though for a more restricted area of the MSSM parameter space. Furthermore,  $A \rightarrow b\bar{b}$  decays of the MSSM pseudoscalar Higgs are always dominant, except at low  $\tan\beta$  and large  $M_A$  (above 200 GeV). Indeed, considering that in the fully hadronic channel, in order to suppress both the effects of combinatorics and of reducible backgrounds (e.g.,  $e^+e^- \rightarrow \gamma^*, Z^* \rightarrow q\bar{q}gggg$  [25]), vertex tagging techniques will certainly be exploited to select  $b\bar{b}$  pairs produced in  $Z$  and  $A$  decays, then it is quite likely that six-quark decays of  $W^\pm$  pairs (with two  $b$ 's) can be a serious noise. Even more so if one further realises that these are irreducible in two respects: not only in the particle content of the final state, but also because they naturally contain a di-jet pair resonating at the  $W^\pm$  mass.

---

<sup>3</sup>Assuming that the mass scale of SUSY partners of ordinary matter is in the TeV range, as preferred by many Grand Unification Theories (GUTs).

### 3 Calculation

In the numerical part of our calculations, as centre-of-mass (CM) energies representative of LEP2 and a future LC, we have used the values  $E_{\text{cm}} = 172$  and  $350, 500$  GeV, respectively. As for the parameters of the theory, we have adopted  $M_Z = 91.17$  GeV,  $\Gamma_Z = 2.516$  GeV,  $M_W = 80.23$  GeV,  $\Gamma_W = 2.2$  GeV,  $\sin^2 \theta_W = 0.23$ ,  $\alpha_{em} = 1/128$  and the two-loop expression for  $\alpha_s$ , with  $\Lambda_{\text{QCD}}^{N_F=5} = 0.200$  GeV. Furthermore, we have kept all quarks massless as a default except the bottom ones (for which we used  $m_b = 4.95$  GeV), in order to speed up the numerical evaluations. (Electron and positron have mass zero too, so have the neutrinos.) In practise, as we neglect Cabibbo-Kobayashi-Maskawa mixing terms (see below, Tab. 3), this corresponds to always neglect the mass along the fermion lines connected to the  $W^\pm$  currents in Fig. 1, while keeping the one of those emerging from the gluon. This should be a good approximation. On the one hand, the energy produced in the  $W^\pm$  decays both at LEP2 and a LC is typically much larger than the quark masses. On the other hand, the latter can give sizable effects in the splitting of the gluon [26]. This approach also naturally allows us to study effects of massive gluinos. As for these, we have spanned their mass  $m_{\tilde{g}}$  over the range 0 to 10 GeV. While doing so, we also have to compare the six-quark and four-quark-two-gluino rates with the four-quark-two-gluon ones. That is, we have to calculate the process  $e^+e^- \rightarrow W^+W^- \rightarrow q\bar{q}q'\bar{q}'gg$ . To do so, we have resorted to the HELAS [27] subroutines, whose results agree with those reported in Ref. [10].

In addition, when  $e^+e^- \rightarrow \text{Higgs } Z \rightarrow W^{+(*)}W^{-(*)}\bar{b}b \rightarrow bb + 4 \text{ jets}$  and  $e^+e^- \rightarrow \Phi A \rightarrow W^{+(*)}W^{-(*)}\bar{b}b \rightarrow bb + 4 \text{ jets}$  have been calculated (at tree-level), where Higgs =  $\phi, \Phi$ , with  $\phi$  the SM scalar boson and  $\Phi = H, h$  the corresponding ones in the MSSM, we have used again heavy  $b$  quarks, with their mass appropriately run up to the mass of the decaying pseudoscalar  $A$  boson in the second process, to match the procedure employed to compute the total widths of the latter [24]. Mass relations and couplings involving the neutral MSSM Higgs bosons have been computed using the full one-loop and the leading two-loop corrections [28], using  $\tan \beta$  and  $M_A$  as inputs, assuming a universal soft Supersymmetry-breaking mass of 1 TeV and negligible mixing in the stop and sbottom mass matrices. To calculate the Higgs cross sections and differential rates we have used the exact  $2 \rightarrow 6$  MEs, including finite width effects of all unstable particles, that we have produced using again the HELAS subroutines.

In order to calculate the Feynman diagrams in Fig. 1 we have used *two* different spinor methods, this enabling us to check the correctness of our results. The first one is based on the formalism of Ref. [29]. A second approach is based on the method developed in Refs. [30, 31, 32]. Since we will express the helicity amplitudes in this last formalism, we will devote some space here to describe its technicalities.

In this method, all spinors for any physical momentum are defined in terms of a basic spinor of an auxiliary light-like momentum. By decomposing the internal momenta in terms of the external ones, using Dirac algebra and rewriting the polarisation of external vectors by means of a spinor current, all amplitudes can eventually be reduced to an algebraic combination of spinors products  $\bar{u}(p_i)u(p_j)$  (with  $i, j, \dots$  labelling the external particles).

- (i) *Spinors*. Since all vector particles entering our calculation eventually splits into fermions,

$\lambda_1 \lambda_3$	$X(p_1, \lambda_1; p_2; p_3, \lambda_3; c_R, c_L)$
++	$(\mu_1 \eta_2 + \mu_2 \eta_1)(c_R \mu_2 \eta_3 + c_L \mu_3 \eta_2) + c_R S(+, p_1, p_2) S(-, p_2, p_3)$
+-	$c_L(\mu_1 \eta_2 + \mu_2 \eta_1) S(+, p_2, p_3) + c_L(c_L \mu_2 \eta_3 + c_R \mu_3 \eta_2) S(+, p_1, p_2)$

Table 1: The  $X$  functions for the two independent helicity combinations in terms of the functions  $S$ ,  $\eta$  and  $\mu$  defined in the text. The remaining  $X$  functions can be obtained by flipping the sign of the helicities and exchanging  $+$  with  $-$  in the  $S$  functions and  $R$  with  $L$  in the chiral coefficients.

$\lambda_1 \lambda_2 \lambda_3 \lambda_4$	$Z(p_1, \lambda_1; p_2, \lambda_2; p_3, \lambda_3; p_4, \lambda_4; c_R, c_L; c'_R, c'_L)$
++++	$-2[S(+, p_3, p_1) S(-, p_4, p_2) c'_R c_R - \mu_1 \mu_2 \eta_3 \eta_4 c'_R c_L - \eta_1 \eta_2 \mu_3 \mu_4 c'_L c_R]$
+++-	$-2\eta_2 c_R [S(+, p_4, p_1) \mu_3 c'_L - S(+, p_3, p_1) \mu_4 c'_R]$
++-+	$-2\eta_1 c_R [S(-, p_2, p_3) \mu_4 c'_L - S(-, p_2, p_4) \mu_3 c'_R]$
+-++	$-2\eta_4 c'_R [S(+, p_3, p_1) \mu_2 c_R - S(+, p_3, p_2) \mu_1 c_L]$
++--	$-2[S(+, p_1, p_4) S(-, p_2, p_3) c'_L c_R - \mu_1 \mu_2 \eta_3 \eta_4 c'_L c_L - \eta_1 \eta_2 \mu_3 \mu_4 c'_R c_R]$
+--+	0
+-+-	$-2[\mu_1 \mu_4 \eta_2 \eta_3 c'_L c_L + \mu_2 \mu_3 \eta_1 \eta_4 c'_R c_R - \mu_2 \mu_4 \eta_1 \eta_3 c'_L c_R - \mu_1 \mu_3 \eta_2 \eta_4 c'_R c_L]$
----	$-2\eta_3 c'_L [S(+, p_2, p_4) \mu_1 c_L - S(+, p_1, p_4) \mu_2 c_R]$

Table 2: The  $Z$  functions for all independent helicity combinations in terms of the functions  $S$ ,  $\eta$  and  $\mu$  defined in the text. The remaining  $Z$  functions can be obtained by flipping the sign of the helicities and exchanging  $+$  with  $-$  in the  $S$  functions and  $R$  with  $L$  in the chiral coefficients.

we only need to introduce the treatment of the spinor fields. External fermions<sup>4</sup> of mass  $m$  and momentum  $p^\mu$  are described by spinors corresponding to states of definite helicity  $\lambda$ ,  $u(p, \lambda)$ <sup>5</sup>, verifying the Dirac equations

$$\not{p} u(p, \lambda) = \pm m u(p, \lambda), \quad \bar{u}(p, \lambda) \not{p} = \pm m \bar{u}(p, \lambda), \quad (1)$$

and the spin sum relation

$$\sum_{\lambda=\pm} u(p, \lambda) \bar{u}(p, \lambda) = \not{p} \pm m, \quad (2)$$

where the sign  $+(-)$  refers (here and in the following) to a particle(antiparticle). One can choose two arbitrary vectors  $k_0$  and  $k_1$  such that

$$k_0 \cdot k_0 = 0, \quad k_1 \cdot k_1 = -1, \quad k_0 \cdot k_1 = 0, \quad (3)$$

and express the spinors  $u(p, \lambda)$  in terms of chiral ones  $w(k_0, \lambda)$  as

$$u(p, \lambda) = w(p, \lambda) + \mu w(k_0, -\lambda), \quad (4)$$

<sup>4</sup>We shall use the term ‘fermion’ and the symbol ‘ $u$ ’ for both particles and antiparticles.

<sup>5</sup>Here,  $p(\lambda)$  represents a generic (anti)spinor four-momentum(helicity).

where

$$w(p, \lambda) = \not{p} w(k_0, -\lambda) / \eta, \quad (5)$$

and

$$\mu = \pm \frac{m}{\eta}, \quad \eta = \sqrt{2|p \cdot k_0|}. \quad (6)$$

The spinors  $w(k_0, \lambda)$  satisfy

$$w(k_0, \lambda) \bar{w}(k_0, \lambda) = \frac{1 + \lambda \gamma_5}{2} \not{k}_0, \quad (7)$$

and therefore

$$\sum_{\lambda=\pm} w(k_0, \lambda) \bar{w}(k_0, \lambda) = \not{k}_0. \quad (8)$$

The phase between chiral states is fixed by

$$w(k_0, \lambda) = \lambda \not{k}_1 w(k_0, -\lambda). \quad (9)$$

The freedom in choosing  $k_0$  and  $k_1$  provides a powerful tool for checking the correctness of any calculation. A convenient, though not unique choice, is the following:  $k_0 = (1, 0, 0, -1)$  and  $k_1 = (0, 1, 0, 0)$ . In such a case the massless spinors in the two methods [29] and [30] coincide exactly, so that it is possible to compare in greater detail the two corresponding numerical codes. In particular, the results obtained with the two formalisms must agree for every single diagram and every polarisation of external particles.

(ii) *The S, X and Z functions.* Using the above definitions one can compute the spinor functions

$$S(\lambda, p_1, p_2) = [\bar{u}(p_1, \lambda) u(p_2, -\lambda)], \quad (10)$$

$$X(p_1, \lambda_1; p_2; p_3, \lambda_3; c_R, c_L) = [\bar{u}(p_1, \lambda_1) \not{p}_2 \Gamma u(p_3, \lambda_3)], \quad (11)$$

and

$$\begin{aligned} Z(p_1, \lambda_1; p_2, \lambda_2; p_3, \lambda_3; p_4, \lambda_4; c_R, c_L; c'_R, c'_L) = \\ [\bar{u}(p_1, \lambda_1) \Gamma^\mu u(p_2, \lambda_2)] [\bar{u}(p_3, \lambda_3) \Gamma'_\mu u(p_4, \lambda_4)], \end{aligned} \quad (12)$$

where

$$\Gamma^{(\prime)\mu} = \gamma^\mu \Gamma^{(\prime)}, \quad (13)$$

and

$$\Gamma^{(\prime)} = c_R^{(\prime)} P_R + c_L^{(\prime)} P_L, \quad (14)$$

with

$$P_R = \frac{1 + \gamma_5}{2}, \quad P_L = \frac{1 - \gamma_5}{2}, \quad (15)$$

the chiral projectors.

By computing the resulting traces one easily finds ( $\varepsilon^{0123} = 1$  is the Levi-Civita tensor) [30, 31]

$$S(+, p_1, p_2) = 2 \frac{(p_1 \cdot k_0)(p_2 \cdot k_1) - (p_1 \cdot k_1)(p_2 \cdot k_0) + i \varepsilon_{\mu\nu\rho\sigma} k_0^\mu k_1^\nu p_1^\rho p_2^\sigma}{\eta_1 \eta_2}, \quad (16)$$

for the  $S$  functions and the expressions listed in Tabs. 1 and 2 for the  $X$  and  $Z$  functions, respectively. For the  $S$  functions, one has  $S(-, p_1, p_2) = S(+, p_2, p_1)^*$ , while the remaining  $X$  and  $Z$  functions can be obtained as described in the captions of Tabs. 1–2.

Other than the spinor parts, to each of the basic amplitudes are associated propagators functions. In the case of off-shell fermions, they have the form

$$D_f(\sum_i p_i) = \frac{1}{(\sum_i p_i)^2 - m_f^2}, \quad (17)$$

whereas in the case of bosons one gets

$$D_V(\sum_i p_i) = \frac{1}{(\sum_i p_i)^2 - M_V^2 + iM_V\Gamma_V}. \quad (18)$$

In eqs. (17)–(18),  $f$  is the flavour  $q, q'$  of a virtual fermion line, whereas  $V = W^\pm, \gamma, Z$  or  $g$ , being  $M_V = \Gamma_V \equiv 0$  if  $V = \gamma$  or  $g$ .

As for the couplings, the notation  $(c_R^{(f)V}, c_L^{(f)V})$  will refer to the pair of chiral indices  $(c_R, c_L)$  of eq. (14) entering in the expressions given in Tabs. 1–2 and associated with the vertex involving a fermion  $f = e, q, q', q''$  (whose label will only appear if the vertex is flavour dependent) and a gauge vector  $V = W^\pm, \gamma, Z, g$ , according to Tab. 3. (Note that we will only need using the flavour-dependent terms  $(c_R^{eV}, c_L^{eV})$ , i.e., for  $f = e$  and  $V = \gamma, Z$ .) For convenience, we also introduce the relative couplings  $g_\gamma = 1$  and  $g_Z = g_\gamma / \tan \theta_W$  entering the  $\gamma W^+ W^-$  and  $Z W^+ W^-$  vertices, respectively, where  $\theta_W$  is the Weinberg angle.

	$\gamma$	$Z$	$W^\pm$	$g$
$c_R$	$Q^f$	$g_R^f / s_W c_W$	0	1
$c_L$	$Q^f$	$g_L^f / s_W c_W$	$1/\sqrt{2}s_W$	1

Table 3: The couplings  $c_R$  and  $c_L$  of eq. (14) for  $u$  and  $d$  type (anti)quarks and electrons/positrons to the gauge bosons  $\gamma, Z, W^\pm$  and  $g$ . One has (adopting the notations  $s_W \equiv \sin \theta_W$  and  $c_W \equiv \cos \theta_W$ )  $g_R^f = -Q^f s_W^2$  and  $g_L^f = T_3^f - Q^f s_W^2$  (with  $q = u, d$ ), where  $(Q^u, T_3^u) = (+\frac{2}{3}, +\frac{1}{2})$ ,  $(Q^d, T_3^d) = (-\frac{1}{3}, -\frac{1}{2})$  and  $(Q^e, T_3^e) = (-1, -\frac{1}{2})$  are the fermion charges and isospins.

We are now ready to present the explicit expressions of the helicity amplitudes associated to our process. To do so, we conventionally assume that initial state momenta are incoming, whereas the final state ones are outgoing. This way, we can define  $-b_i = b_j = 1$ , where  $i = 1, 2$  and  $j = 3, \dots, 8$ , so that  $\sum_{k=1, \dots, 8} b_k p_k = 0$ . In correspondence to the graphs in Figs. 1, one can write the Feynman amplitude squared, summed/averaged over final/initial colours and spin, as

$$|M|^2 = \frac{g_s^2 e^4}{4} \sum_{\{\lambda\}} \sum_{i=1}^8 \sum_{j=1}^8 C_{ij} T_i(\{\lambda\}) T_j^*(\{\lambda\}), \quad (19)$$

where  $C_{ij}$  are the colour factors (see below) and with  $\sum_{\{\lambda\}}$  referring to a summation over all possible combinations of the helicities  $\lambda_1, \dots, \lambda_8$  of the external particles. The quantities  $g_s$  and

$e$  are related to the aforementioned couplings by the usual relations  $g_s^2 \equiv 4\pi\alpha_s$  and  $e^2 \equiv 4\pi\alpha_{em}$  (in natural units). Assuming, for sake of illustration, that the process (via  $W^+W^-$ )

$$\boxed{e^+(p_1, \lambda_1) \ e^-(p_2, \lambda_2) \longrightarrow \ u(p_3, \lambda_3) \ \bar{d}(p_4, \lambda_4) \ s(p_5, \lambda_5) \ \bar{c}(p_6, \lambda_6) \ b(p_7, \lambda_7) \ \bar{b}(p_8, \lambda_8)}$$

has to be calculated, then the helicity amplitudes  $T_i$  can be written as

$$\begin{aligned} T_1(\{\lambda\}) &= -D_g(p_7 + p_8)D_W(p_3 + p_4 + p_7 + p_8)D_W(p_5 + p_6) \\ &\quad D_u(p_3 + p_7 + p_8)D_{\nu_e}(p_2 - p_5 - p_6) \\ &\quad \sum_{i=3,7,8} \sum_{j=2,5,6} b_i b_j \sum_{\lambda=\pm} \sum_{\lambda'=\pm} \\ &\quad Z(p_7, \lambda_7; p_8, -\lambda_8; p_3, \lambda_3; p_i, \lambda; c_R^g, c_L^g; c_R^g, c_L^g) \\ &\quad Z(p_i, \lambda; p_4, -\lambda_4; p_1, \lambda_1; p_j, \lambda'; c_R^W, c_L^W; c_R^W, c_L^W) \\ &\quad Z(p_j, \lambda'; p_2, -\lambda_2; p_5, \lambda_5; p_6, -\lambda_6; c_R^W, c_L^W; c_R^W, c_L^W), \end{aligned} \quad (20)$$

$$\begin{aligned} T_2(\{\lambda\}) &= +D_g(p_7 + p_8)D_W(p_3 + p_4 + p_7 + p_8)D_W(p_5 + p_6) \\ &\quad D_d(p_4 + p_7 + p_8)D_{\nu_e}(p_2 - p_5 - p_6) \\ &\quad \sum_{i=4,7,8} \sum_{j=2,5,6} b_i b_j \sum_{\lambda=\pm} \sum_{\lambda'=\pm} \\ &\quad Z(p_7, \lambda_7; p_8, -\lambda_8; p_i, \lambda; p_4, -\lambda_4; c_R^g, c_L^g; c_R^g, c_L^g) \\ &\quad Z(p_3, \lambda_3; p_i, \lambda; p_1, \lambda_1; p_j, \lambda'; c_R^W, c_L^W; c_R^W, c_L^W) \\ &\quad Z(p_j, \lambda'; p_2, -\lambda_2; p_5, \lambda_5; p_6, -\lambda_6; c_R^W, c_L^W; c_R^W, c_L^W), \end{aligned} \quad (21)$$

$$\begin{aligned} T_3(\{\lambda\}) &= +D_g(p_7 + p_8)D_W(p_3 + p_4)D_W(p_5 + p_6 + p_7 + p_8) \\ &\quad D_s(p_5 + p_7 + p_8)D_{\nu_e}(p_1 - p_3 - p_4) \\ &\quad \sum_{i=5,7,8} \sum_{j=1,3,4} b_i b_j \sum_{\lambda=\pm} \sum_{\lambda'=\pm} \\ &\quad Z(p_7, \lambda_7; p_8, -\lambda_8; p_5, \lambda_5; p_i, \lambda; c_R^g, c_L^g; c_R^g, c_L^g) \\ &\quad Z(p_i, \lambda; p_6, -\lambda_6; p_j, \lambda'; p_2, -\lambda_2; c_R^W, c_L^W; c_R^W, c_L^W) \\ &\quad Z(p_1, \lambda_1; p_j, \lambda'; p_3, \lambda_3; p_4, -\lambda_4; c_R^W, c_L^W; c_R^W, c_L^W), \end{aligned} \quad (22)$$

$$\begin{aligned} T_4(\{\lambda\}) &= -D_g(p_7 + p_8)D_W(p_3 + p_4)D_W(p_5 + p_6 + p_7 + p_8) \\ &\quad D_c(p_6 + p_7 + p_8)D_{\nu_e}(p_1 - p_3 - p_4) \\ &\quad \sum_{i=6,7,8} \sum_{j=1,3,4} b_i b_j \sum_{\lambda=\pm} \sum_{\lambda'=\pm} \\ &\quad Z(p_7, \lambda_7; p_8, -\lambda_8; p_i, \lambda; p_6, -\lambda_6; c_R^g, c_L^g; c_R^g, c_L^g) \\ &\quad Z(p_5, \lambda_5; p_i, \lambda; p_j, \lambda'; p_2, -\lambda_2; c_R^W, c_L^W; c_R^W, c_L^W) \\ &\quad Z(p_1, \lambda_1; p_j, \lambda'; p_3, \lambda_3; p_4, -\lambda_4; c_R^W, c_L^W; c_R^W, c_L^W), \end{aligned} \quad (23)$$

$$\begin{aligned}
T_5(\{\lambda\}) &= +D_g(p_7 + p_8)D_W(p_3 + p_4 + p_7 + p_8)D_W(p_5 + p_6) \\
&\quad D_u(p_3 + p_7 + p_8) \sum_{V=\gamma,Z} g_V D_V(p_1 + p_2) \\
&\quad \sum_{i=3,7,8} b_i \sum_{\lambda=\pm} \\
&\quad \{Z(p_1, \lambda_1; p_2, -\lambda_2; p_i, \lambda; p_4, -\lambda_4; c_R^{eV}, c_L^{eV}; c_R^W, c_L^W) \\
&\quad [ \sum_{j=3,4,7,8} b_j X(p_5, \lambda_5; p_j; p_6, -\lambda_6; c_R^W, c_L^W) - \\
&\quad \sum_{j=1,2} b_j X(p_5, \lambda_5; p_j; p_6, -\lambda_6; c_R^W, c_L^W) ] + \\
&\quad Z(p_i, \lambda; p_4, -\lambda_4; p_5, \lambda_5; p_6, -\lambda_6; c_R^W, c_L^W; c_R^W, c_L^W) \\
&\quad [ \sum_{j=5,6} b_j X(p_1, \lambda_1; p_j; p_2, -\lambda_2; c_R^{eV}, c_L^{eV}) - \\
&\quad \sum_{j=3,4,7,8} b_j X(p_1, \lambda_1; p_j; p_2, -\lambda_2; c_R^{eV}, c_L^{eV}) ] + \\
&\quad Z(p_5, \lambda_5; p_6, -\lambda_6; p_1, \lambda_1; p_2, -\lambda_2; c_R^W, c_L^W; c_R^{eV}, c_L^{eV}) \\
&\quad [ \sum_{j=1,2} b_j X(p_i, \lambda; p_j; p_4, -\lambda_4; c_R^W, c_L^W) - \\
&\quad \sum_{j=5,6} b_j X(p_i, \lambda; p_j; p_4, -\lambda_4; c_R^W, c_L^W) ] \} \\
&\quad Z(p_7, \lambda_7; p_8, -\lambda_8; p_3, \lambda_3; p_i, \lambda; c_R^g, c_L^g; c_R^g, c_L^g),
\end{aligned} \tag{24}$$

$$\begin{aligned}
T_6(\{\lambda\}) &= -D_g(p_7 + p_8)D_W(p_3 + p_4 + p_7 + p_8)D_W(p_5 + p_6) \\
&\quad D_d(p_4 + p_7 + p_8) \sum_{V=\gamma,Z} g_V D_V(p_1 + p_2) \\
&\quad \sum_{i=4,7,8} b_i \sum_{\lambda=\pm} \\
&\quad \{Z(p_1, \lambda_1; p_2, -\lambda_2; p_3, \lambda_3; p_i, \lambda; c_R^{eV}, c_L^{eV}; c_R^W, c_L^W) \\
&\quad [ \sum_{j=3,4,7,8} b_j X(p_5, \lambda_5; p_j; p_6, -\lambda_6; c_R^W, c_L^W) - \\
&\quad \sum_{j=1,2} b_j X(p_5, \lambda_5; p_j; p_6, -\lambda_6; c_R^W, c_L^W) ] + \\
&\quad Z(p_3, \lambda_3; p_i, \lambda; p_5, \lambda_5; p_6, -\lambda_6; c_R^W, c_L^W; c_R^W, c_L^W) \\
&\quad [ \sum_{j=5,6} b_j X(p_1, \lambda_1; p_j; p_2, -\lambda_2; c_R^{eV}, c_L^{eV}) - \\
&\quad \sum_{j=3,4,7,8} b_j X(p_1, \lambda_1; p_j; p_2, -\lambda_2; c_R^{eV}, c_L^{eV}) ] + \\
&\quad Z(p_5, \lambda_5; p_6, -\lambda_6; p_1, \lambda_1; p_2, -\lambda_2; c_R^W, c_L^W; c_R^{eV}, c_L^{eV}) \\
&\quad [ \sum_{j=1,2} b_j X(p_3, \lambda_3; p_j; p_i, \lambda; c_R^W, c_L^W) - \\
&\quad \sum_{j=1,2} b_j X(p_3, \lambda_3; p_j; p_i, \lambda; c_R^W, c_L^W) ] \}
\end{aligned} \tag{25}$$

$$\sum_{j=5,6} b_j X(p_3, \lambda_3; p_j; p_i, \lambda; c_R^W, c_L^W)]\} \\ Z(p_7, \lambda_7; p_8, -\lambda_8; p_i, \lambda; p_4, -\lambda_4; c_R^g, c_L^g; c_R^g, c_L^g),$$

$$\begin{aligned} T_7(\{\lambda\}) &= -D_g(p_7 + p_8)D_W(p_3 + p_4)D_W(p_5 + p_6 + p_7 + p_8) \\ &\quad D_s(p_5 + p_7 + p_8) \sum_{V=\gamma, Z} g_V D_V(p_1 + p_2) \\ &\quad \sum_{i=5,7,8} b_i \sum_{\lambda=\pm} \\ &\quad \{Z(p_1, \lambda_1; p_2, -\lambda_2; p_i, \lambda; p_6, -\lambda_6; c_R^{eV}, c_L^{eV}; c_R^W, c_L^W) \\ &\quad [ \sum_{j=5,6,7,8} b_j X(p_3, \lambda_3; p_j; p_4, -\lambda_4; c_R^W, c_L^W) - \\ &\quad \sum_{j=1,2} b_j X(p_3, \lambda_3; p_j; p_4, -\lambda_4; c_R^W, c_L^W)] + \\ &\quad Z(p_i, \lambda; p_6, -\lambda_6; p_3, \lambda_3; p_4, -\lambda_4; c_R^W, c_L^W; c_R^W, c_L^W) \\ &\quad [ \sum_{j=3,4} b_j X(p_1, \lambda_1; p_j; p_2, -\lambda_2; c_R^{eV}, c_L^{eV}) - \\ &\quad \sum_{j=5,6,7,8} b_j X(p_1, \lambda_1; p_j; p_2, -\lambda_2; c_R^{eV}, c_L^{eV})] + \\ &\quad Z(p_3, \lambda_3; p_4, -\lambda_4; p_1, \lambda_1; p_2, -\lambda_2; c_R^W, c_L^W; c_R^{eV}, c_L^{eV}) \\ &\quad [ \sum_{j=1,2} b_j X(p_i, \lambda; p_j; p_6, -\lambda_6; c_R^W, c_L^W) - \\ &\quad \sum_{j=3,4} b_j X(p_i, \lambda; p_j; p_6, -\lambda_6; c_R^W, c_L^W)]\} \\ &\quad Z(p_7, \lambda_7; p_8, -\lambda_8; p_5, \lambda_5; p_i, \lambda; c_R^g, c_L^g; c_R^g, c_L^g), \end{aligned} \tag{26}$$

$$\begin{aligned} T_8(\{\lambda\}) &= +D_g(p_7 + p_8)D_W(p_3 + p_4)D_W(p_5 + p_6 + p_7 + p_8) \\ &\quad D_c(p_6 + p_7 + p_8) \sum_{V=\gamma, Z} g_V D_V(p_1 + p_2) \\ &\quad \sum_{i=6,7,8} b_i \sum_{\lambda=\pm} \\ &\quad \{Z(p_1, \lambda_1; p_2, -\lambda_2; p_5, \lambda_5; p_i, \lambda; c_R^{eV}, c_L^{eV}; c_R^W, c_L^W) \\ &\quad [ \sum_{j=5,6,7,8} b_j X(p_3, \lambda_3; p_j; p_4, -\lambda_4; c_R^W, c_L^W) - \\ &\quad \sum_{j=1,2} b_j X(p_3, \lambda_3; p_j; p_4, -\lambda_4; c_R^W, c_L^W)] + \\ &\quad Z(p_5, \lambda_5; p_i, \lambda; p_3, \lambda_3; p_4, -\lambda_4; c_R^W, c_L^W; c_R^W, c_L^W) \\ &\quad [ \sum_{j=3,4} b_j X(p_1, \lambda_1; p_j; p_2, -\lambda_2; c_R^{eV}, c_L^{eV}) - \end{aligned} \tag{27}$$

$$\begin{aligned}
& \sum_{j=5,6,7,8} b_j X(p_1, \lambda_1; p_j; p_2, -\lambda_2; c_R^{eV}, c_L^{eV})] + \\
& Z(p_3, \lambda_3; p_4, -\lambda_4; p_1, \lambda_1; p_2, -\lambda_2; c_R^W, c_L^W; c_R^{eV}, c_L^{eV}) \\
& [ \sum_{j=1,2} b_j X(p_5, \lambda_5; p_j; p_i, \lambda; c_R^W, c_L^W) - \\
& \sum_{j=3,4} b_j X(p_5, \lambda_5; p_j; p_i, \lambda; c_R^W, c_L^W) ] \} \\
& Z(p_7, \lambda_7; p_8, -\lambda_8; p_i, \lambda; p_6, -\lambda_6; c_R^g, c_L^g; c_R^g, c_L^g).
\end{aligned}$$

Concerning the colour factors, there are basically only two of these, if the flavours in the final state are all different. They are (hereafter,  $N_C = 3$ ):  $C_{ij} = \frac{N_C}{4}(N_C^2 - 1) = 6$ , if  $i$  and  $j$  are diagrams in which the gluon emission takes place from the same  $W^\pm$ , and  $C_{ij} = 0$  otherwise (because of colour conservation)<sup>6</sup>.

If one or two quark flavours in the final state are identical, then the number of Feynman graphs proliferates, as explained in Sect. 2. The spinor part of the additional diagrams can easily be obtained by interchanging the labels of identical particles in the above formulae, factorising a minus sign for each of these operations. In addition, as many factors of the form  $\frac{1}{2^n}$  multiply the amplitude squared as the number of  $n$ -tuple of identical final state particles. As for the new colour factors, one has to do some more work. However, it is rather trivial to realise than only the following colour structures need to be computed<sup>7</sup>:

$$\begin{aligned}
\text{Circle} &= N_C = 3 \\
\text{Two Circles with Two Wavy Lines} &= (N_C^2 - 1)/4 = 2
\end{aligned}$$

<sup>6</sup>In other terms, ‘perturbative’ colour-rearrangement is not possible in  $W^+W^- \rightarrow 6$  quarks at  $\mathcal{O}(\alpha_s^2)$ , contrary to the case of four-quark-two-gluon decays at the same order [10].

<sup>7</sup>The product of the first two yields the factor  $C_{ij} = 6$  mentioned above whereas the third produces the other one,  $C_{ij} = 0$ .

$$= 0$$

$$= (1/N_C - N_C)/4 = -2/3$$

$$= (1/N_C - 2N_C + N_C^3)/4 = 16/3$$

$$= 0$$

Since the all procedure is quite cumbersome, we refrain here from building up explicitly the correct MEs for identical flavours by combining the above colour factors (and their products) with the appropriate interferences among spinor amplitudes. Instead, we make available upon request our programs, that do include the described implementation.

Before proceeding further, we would now like to devote some space to describe the procedure adopted to integrate the squared amplitude in eq. (19). In fact, in order to deal numerically with the non-trivial resonant structure of our six-quark process, one has to apply some special care. Here, we have adopted the technique of splitting the ME in a sum of non-gauge-invariant pieces, each of these implementing a different resonant structure, and of integrating them separately with the appropriate mapping of the phase space variables.

Things go as follows. Firstly, one isolates the diagrams with similar resonant structure by grouping these together in ‘subamplitudes’. From the graphs in Fig. 1, one can recognise the following two resonant structures: say, (a)  $W^+ \rightarrow (3478)$  and  $W^- \rightarrow (56)$  (graphs 1,2,5,6, so that  $T_a = \sum_{i=1,2,5,6} T_i$ ); (b)  $W^+ \rightarrow (34)$  and  $W^- \rightarrow (5678)$  (graphs 3,4,7,8, so that  $T_b = \sum_{i=3,4,7,8} T_i$ ). Secondly, one defines the mentioned non-gauge-invariant components of the amplitude squared,

by appropriately combining the subamplitudes. For example, we have simply taken the square of the two resonant subamplitudes and their interference:  $|T_a|^2$ ,  $|T_b|^2$  and  $2 \text{Real}(T_a T_b^*)$ , respectively. Thirdly, one maps the phase space around the resonances. Fourthly, the various amplitude squared terms are integrated separately and added up in the end (to recover gauge invariance) to produce total and differential cross sections. In this respect, we would like to mention that all results presented here have been obtained by resorting to the adaptive multi-dimensional integrator **VEGAS** [33], and they have been counter-checked against the outputs of the multi-particle phase space generator **RAMBO** [34].

## 4 Results

In order to select a six-‘jet’ sample we apply a jet clustering algorithm directly to the ‘quarks’ in the final state of  $e^+e^- \rightarrow W^+W^- \rightarrow q\bar{q}q'\bar{q}''q''\bar{q}''$ . For illustrative purposes, we use the Durham jet-finder [35] only. However, we remark that none of the main features of our analysis depends drastically on such a choice. This algorithm is based on the ‘(squared) transverse-momentum’ measure

$$y_{ij} = \frac{2 \min(E_i^2, E_j^2)(1 - \cos \theta_{ij})}{s}, \quad (28)$$

where  $E_i$  and  $E_j$  are the energies and  $\theta_{ij}$  the separation of any pair  $ij$  of particles in the final state, with  $3 \leq i < j = 4, \dots, 8$ , to be compared against a resolution parameter denoted by  $y_{\text{cut}}$ . In our tree-level studies, the selected rate is then nothing else than the total partonic cross section with a cut  $y_{ij} > y_{\text{cut}}$  on any possible  $ij$  combination.

Fig. 2 presents the total cross section at LEP2 (above) and a LC (below) for six-quark events as a function of the resolution, with and without the correlations described in Sect. 2. (A summation over all possible combinations of quark flavours has been performed.) We see a large effect on the integrated rates. Indeed, the ratio between the two curves is about 1.6 for  $y_{\text{cut}} \lesssim 0.01$  at both energies. The cross section including the interference effects is indeed smaller, in accordance with the fact that these are generally destructive.

Six-quark decays of  $W^+W^-$  pairs are detectable but not numerous at  $E_{\text{cm}} = 172$  GeV for  $y_{\text{cut}} \lesssim 0.004$ , assuming 500 inverse picobarn of luminosity. At the minimum  $y_{\text{cut}}$  considered here and for the mentioned figure of  $\int \mathcal{L} dt$  some 8 events should be expected. In contrast, at a LC running at the top-antitop threshold, i.e.,  $E_{\text{cm}} \approx 2m_t \approx 350$  GeV, assuming 100 to 500  $\text{fb}^{-1}$  per year (e.g., in the TESLA design), one gets between 100 and 500 events, for  $y_{\text{cut}} = 0.001$ . Presumably, a QCD  $K$ -factor of order 1.5–2 should apply to the total production rates of  $e^+e^- \rightarrow W^+W^- \rightarrow q\bar{q}q'\bar{q}''q''\bar{q}''$ , in line with the results obtained for  $e^+e^- \rightarrow \gamma^*, Z \rightarrow q\bar{q}q'\bar{q}'$  [36], so that the actual number of events detected should accordingly be larger.

As for effects of  $W^+W^- \rightarrow 6$  quark events onto the line-shape of the  $W^\pm$  mass resonance, we have found these negligible. We have performed **MINUIT** [37] fits of the form

$$f(m) = c_1 \frac{c_2^2 c_3^2}{(m^2 - c_2^2)^2 + c_2^2 c_3^2} + g(m), \quad (29)$$

where the term  $g(m)$  is meant to simulate a smooth background due to mis-assigned jets induced

by the jet-clustering algorithm,

$$g(m) = \begin{cases} 0, \\ c_4 + c_5 (m - c_2) + c_6 (m - c_2)^2, \\ c_4 \frac{1}{1 + \exp((m - c_5)/c_6)}, \end{cases} \quad (30)$$

that is, a null, a three-term polynomial and a smeared step function, see Ref. [3]. Clearly, in eq. (29), we have assumed a Breit-Wigner shape characterised by a peak height  $c_1$ , a position  $c_2$  and a width  $c_3$ , these corresponding to the normalisation,  $M_W$  and  $\Gamma_W$ , respectively. By adopting various algorithms and resolutions, we have never found a difference larger than 10 MeV between the  $c_2$  coefficients obtained from various pairs of mass spectra  $m$  (one computed with and the other without the mentioned correlations), neither at LEP2 nor at a LC. Fig. 3 illustrates typical differences, e.g., in the case of an ‘average mass’. This can be obtained by applying the Durham algorithm with  $y_{\text{cut}} = 0.001$  to the  $2 \rightarrow 6$  process  $e^+e^- \rightarrow W^+W^- \rightarrow q\bar{q}q'\bar{q}'q''\bar{q}''$  and then forcing the six-body final state into a four-body one, by clustering the three softest particles  $i, j, k$  into one pseudo-particle  $l$  with four-momentum  $p_l^\mu = p_i^\mu + p_j^\mu + p_k^\mu$  (the so-called ‘E recombination scheme’ [3]). Having done this, one looks at the three possible pairs of di-jet combinations that can be formed out of the four surviving four-momenta, rejects the one in which the two most energetic particles are put together and plots the average of the other two,  $M_{\text{ave}}$ .

We will now proceed to studying the relevance of  $e^+e^- \rightarrow W^+W^- \rightarrow q\bar{q}q'\bar{q}'q''\bar{q}''$  events in the search for new particles at LEP2 and a LC. In doing so, we will use the full ME, with all mentioned correlations included. For a start, we have found it rather easy to individuate four particle momenta out of the original six in the final state that preserve the typical differences between (on the one hand) gluons and (on the other hand) quarks and gluinos in the variables which are used to fit the QCD colour factors (see Footnote 1). This can be verified by referring to Fig. 4, where the differential distributions (normalised to unity) in the four variables<sup>8</sup>

1. the Bengtsson-Zerwas angle  $\chi_{\text{BZ}}$ ;
2. the (modified) Körner-Schierholz-Willrodt angle  $\Phi_{\text{KSW}}^*$ ;
3. the (modified) Nachtmann-Reiter angle  $\theta_{\text{NR}}^*$ ;
4. the angle between the two least energetic jets  $\theta_{34}$ ;

have been plotted for  $e^+e^- \rightarrow W^+W^- \rightarrow q\bar{q}q'\bar{q}'gg$  and  $e^+e^- \rightarrow W^+W^- \rightarrow q\bar{q}q'\bar{q}'\tilde{g}\tilde{g}$  events, e.g., at LEP2<sup>9</sup>. Here, for reference, the gluino mass has been set equal to one (usual jet-finder and resolution have been used). The above four-particle quantities have been built by simply using the four three-momenta that survive after having removed the pair which yields the invariant mass closer to  $M_W$ .

As for the total rates of the various six-jet contributions, these can be found in Fig. 5. The CM energies are the same as in Fig. 2. It is clear from the LEP2 plot that at such a collider

<sup>8</sup>See, e.g., Ref. [38] for the definition of the angles and for some typical spectra in the case of  $e^+e^- \rightarrow 4$  parton processes at the  $Z$  peak.

<sup>9</sup>Those for  $e^+e^- \rightarrow W^+W^- \rightarrow q\bar{q}q'\bar{q}'q''\bar{q}''$  coincide within numerical errors with the latter.

there is no chance of selecting a statistically significant sample of SUSY events. If one assumes, say, 500 inverse picobarn to be collected at LEP2, then, from looking at the upper part of Fig. 5, it follows that the number of SUSY events produced should be between 1 and 8, for  $y_{\text{cut}} = 0.001$  in the Durham algorithm, depending on the actual value of the gluino mass ! In contrast, one should expect a LC to be an excellent laboratory for gluino searches in  $W^+W^-$  decays. (Incidentally, notice that at a LC the cross section for  $W^+W^-$  production is even larger than that for the  $Z$ .) In fact, although the LC production rate of  $e^+e^- \rightarrow W^+W^-$  is smaller than the LEP2 one, the instantaneous luminosity is in contrast much higher, since some 100 to 500  $\text{fb}^{-1}$  of data per annum are expected to be collected. If one goes back to the lower part of Fig. 5 and considers a LC running at 350 GeV, then one should expect to produce approximately 120 to 600 events per year with very light gluinos, for  $y_{\text{cut}} = 0.001$  in the Durham scheme (possibly, twice as much, accounting for the  $K$ -factor).

Varying the CM energy of the colliding  $e^+e^-$  beams has little effects on the effectiveness of our simple procedure based on the  $M_W$  selection of four four-momenta. This can be seen by defining the Lorentz-invariant (contrary to angles) quantity

$$V = N_V \frac{\varepsilon(p_1, p_2, p_3, p_4)}{s^2}, \quad (31)$$

where the numerator represents the contraction of the jet four-momenta  $p_1^\mu, p_2^\nu, p_3^\rho, p_4^\sigma$  used in Fig. 4 with the Levi-Civita tensor  $\varepsilon_{\mu\nu\rho\sigma}$  of Sect. 3 and where the factor  $N_V$  has been introduced for scaling purposes. The quantity in eq. (31) is presented in Fig. 6, e.g., for  $E_{\text{cm}} = 172$  GeV, using  $N_V = 1000$ : compare to Fig. 4, where the same energy was used. In this case, we again have looked at the four-quark-two-gluon and four-quark-two-gluino final states only, as the six-quark contribution behaves rather similarly to the SUSY one. Basically,  $V$  is a measure of the acoplanarity of the event [39], this in turn quantifying the relative orientation of the planes spanned by, on the one hand, the two most energetic particles and, on the other hand, the two least energetic ones. In fact, it should be recalled that the first three angles introduced above are nothing else than a different way of describing the helicity property that in a  $g^* \rightarrow gg$  splitting the two gluons (they are spin 1 bosons) tend to lie in the same plane of the two quarks which originally emitted the virtual gluon, whereas in  $g^* \rightarrow q\bar{q}$  and  $g^* \rightarrow \tilde{g}\tilde{g}$  splittings the two quarks and the two gluinos (they are both spin 1/2 fermions) tend to be in a perpendicular one. Fig. 6 eloquently confirms this dynamics.

Under these circumstances then, dedicated analyses in the angular variables of Fig. 4 could well be attempted at a LC (also notice the somewhat improved ‘SUSY to ordinary QCD’ production ratio respect to LEP2). To select a six-jet sample from  $W^+W^-$  decays should be rather straightforward, we believe, by removing those where none of the di-jet invariant masses reproduce  $M_W$ , most of which would come from  $\mathcal{O}(\alpha_s^4)$  QCD events [25], and those in which one or more three-jet masses reconstruct  $m_t = 175$  GeV, as it occurs in single- and double-top events [40]. In principle, one could also resort to semileptonic decays, i.e.,  $W^+W^- \rightarrow 2$  jets  $\ell^\pm$  plus missing energy. In practise, though, the loss of kinematic constraints, because of the neutrino escaping detection, would render the background suppression less effective. Furthermore, to exploit the sort of vertex tagging procedure described in Ref. [22] and recalled in Sect. 2 could be even more fruitful, given the high efficiency and purity foreseen for such a technique by the time the electron-positron linear colliders will have started operation, but provided that

$\tau_{\tilde{g}} \sim \frac{M_{\tilde{g}}^4}{\alpha_{em}\alpha_s m_{\tilde{g}}^5} \gtrsim \tau_b$  (e.g., in the SUGRA scenario), with  $\tau_b \sim 1.6 \cdot 10^{-12}$  sec and where  $M_{\tilde{g}}$  is the typical squark mass.

We now turn our attention to the case of Higgs searches in the  $bb + 4$  jet channel, at a LC<sup>10</sup>. Though  $e^+e^- \rightarrow W^+W^- \rightarrow q\bar{q}q'\bar{q}'b\bar{b}$  events can be relevant as background processes in both the SM and the MSSM, for reasons of space, we illustrate here the phenomenology of the latter model only. The former case can easily be dealt with by the reader itself, by referring to the specialised bibliography on the subject [41].

Fig. 7 presents the Higgs rates at a LC with  $E_{cm} = 350$  (above) and 500 (below) GeV, for two reference values of  $\tan\beta$ , 3.0 and 30., as a function of the scalar Higgs masses. The background considered here clearly does not depend on either of them, so it is simply indicated by an arrow in both plots, in correspondence of the transition value of the Higgs mass between the light,  $M_h$ , and heavy,  $M_H$ , regime. As usual, six-jet final states (here, with two  $b$  quarks) are selected using the Durham jet-finder with cut-off  $y_{cut} = 0.001$ . For such jet selection enforced, the background overwhelms both scalar Higgs signals,  $e^+e^- \rightarrow \Phi Z$  and  $e^+e^- \rightarrow \Phi A$ , over a large interval in  $M_h$  and  $M_H$ .

However, the situation is in reality less dramatic than it would appear from Fig. 7 only, if one refers to Fig. 8 too. In fact, whereas all the decay products emerging from the  $W^+W^-Z$  and  $W^+W^-A$  intermediate states of the Higgs signals are naturally energetic and far apart, the  $b$  quarks generated in  $W^+W^-$  events tend to be soft and collinear, owing to the dominant infrared dynamics of the gluon splitting (see the dashed lines in the top plots of Figs. 10 and 12 below). In other terms, whereas to increase the value of  $y_{cut}$  would affect both signals only slightly, this is no longer true for the background. In fact, in one increases the resolution, e.g., by a factor of five, to  $y_{cut} = 0.005$ , the latter decreases by a factor of about 90(25) at  $E_{cm} = 350(500)$  GeV. In correspondence, the typical loss for each of the former is less than a factor of 5 at both energies.

Therefore, even in those cases where the background is apparently well above the signal, e.g. for  $M_A = 220$  GeV and  $\tan\beta = 3.0$  GeV (corresponding to  $M_H \approx 230$  GeV), the latter being dominated at 350 GeV by  $HZ \rightarrow W^+W^-Z$  production and decay (the asterisk in the upper frame of Fig. 7), a judicious choice of  $y_{cut}$  combined with a dedicate selection in  $M_{ij}$  (with  $i < j = 1, \dots, 4$ , the six di-jet invariant masses that can be reconstructed from the light quark jets ordered in energy, see Fig. 9) and  $M_{b\bar{b}}$  (that of the two  $b$  jets, see top frame of Fig. 10) around the  $W^\pm$  and  $Z$  masses, respectively, might allow for the remotion of  $e^+e^- \rightarrow W^+W^- \rightarrow q\bar{q}q'\bar{q}'b\bar{b}$  events in the spectrum of the four-light-quark invariant mass, in which the Higgs peak generated in the production and decay sequence  $e^+e^- \rightarrow HZ \rightarrow W^+W^-Z \rightarrow q\bar{q}q'\bar{q}'b\bar{b}$  should appear (bottom frame of Fig. 10). (Notice that bins are there two GeV wide, being the expected  $M_{4q}$  resolution more realistically, say, five times as large, so that the signal would actually be well below the background in this distribution, after jet-selection cuts only.) However, even for  $\int \mathcal{L} dt = 500 \text{ fb}^{-1}$ , the event rate is rather poor in this case, about four events per year.

In contrast, for other settings of the MSSM parameter spaces, the signal would clearly be

---

<sup>10</sup>Notice that in all forthcoming plots we have not included a multiplicative factor  $\epsilon_b^2$ , accounting for the finite efficiency of tagging the two heavy quarks. We assume  $\epsilon_b$  to be large enough so that the reducible background from  $e^+e^- \rightarrow W^+W^- \rightarrow q\bar{q}q'\bar{q}'gg$  studied in Ref. [10] and in the first part of this Section can easily be filtered out of the  $bb + 4$  jet sample.

visible above the QCD noise considered here, even before the implementation of the Higgs selection cuts. As illustrative example, we consider again the same point,  $M_A = 220$  GeV and  $\tan\beta = 3.0$  GeV ( $M_H \approx 230$  GeV), but at 500 GeV, where the dominant Higgs channel now involves  $HA \rightarrow W^+W^-A$  production and decay (see the asterisk in the bottom plot of Fig. 7). For such a choice, the  $M_W$  resonance is already much higher for the signal than for the background (see Fig. 11, where the arrows denote the height of the peaks for the latter) and both the  $A$  and  $H$  Breit-Wigner shapes clearly stick out in the  $M_{b\bar{b}}$  and  $M_{4q}$  spectra, respectively (see Fig. 12), even if the four-jet mass resolution is much larger than 2 GeV. In this case, the yearly production rate of the signal would be 140 events (again, assuming  $\int \mathcal{L} dt = 500 \text{ fb}^{-1}$ ).

The discussion for the case of the light scalar Higgs of the MSSM is rather similar, so we do not repeat it here. In this case, in general, the MSSM parameter space accessible via the Higgs signature  $h \rightarrow W^+W^- \rightarrow 4$  jets is much reduced though, as only a light scalar with mass at the very upper hand of its allowed range can decay in such a channel (in which one of the two  $W^\pm$  bosons is off-shell): see Fig. 7.

## 5 Conclusions

In the end,  $\mathcal{O}(\alpha_s^2)$  decays into six-fermions of  $W^+W^-$  pairs produced in  $e^+e^-$  scatterings can be detected at LEP2 and a LC as well, the latter with  $350 \text{ GeV} \lesssim E_{\text{cm}} \lesssim 500 \text{ GeV}$ . At both colliders though, they have little relevance in  $M_W$  measurements. As for New Physics analyses, such events can be important in a LC environment. Firstly, they can produce very light gluinos at statistically significant rate. These sparticles have survived the LEP constraints and in some SUSY scenarios could well be the next-to-lightest ones, all other being much heavier. The new SUSY signals could be searched for in six-jet samples in which only two of the jets reconstruct the  $W^\pm$  mass. Using the remaining four-jet subset one could either fit the QCD colour factors to the shape of some typical angular distributions or exploit the tagging of a displaced vertex. Secondly, they can represent an overwhelming background in the search for Higgs bosons, both in the SM and in the MSSM, produced via  $e^+e^- \rightarrow$  Higgs  $Z \rightarrow W^+W^-Z$  and  $e^+e^- \rightarrow \Phi A \rightarrow W^+W^-A$ , where Higgs =  $\phi, \Phi$  and  $\Phi = H, h$  are the scalar particles and in which  $W^+W^- \rightarrow 4$  (light) jets. However, to cut around the  $Z$  and/or  $A$  masses in the  $b\bar{b}$  subsystem, should in general allow one to reduce drastically such a QCD noise in the Higgs candidate sample of six-jets with two displaced vertices, provided a high  $b$  tagging efficiency can be achieved.

The calculation of the exact matrix element for the  $2 \rightarrow 6$  process  $e^+e^- \rightarrow W^+W^- \rightarrow q\bar{q}q'\bar{q}'q''\bar{q}''$  through the order  $\mathcal{O}(\alpha_{em}^4\alpha_s^2)$  has been performed by means of helicity amplitude methods. This has led to compact analytic expressions of the MEs and to their fast implementation in a FORTRAN code which can profitably be exploited in high statistic MC simulations.

## Acknowledgements

SM is grateful to the UK PPARC for support and to the Theoretical Physics Department of the University of Granada for kind hospitality while part of this work was carried out. Many useful discussions with Ramon Muoz-Tapia during the earlier stages of this work are kindly

acknowledged.

## References

- [1] L. Lönnblad and T. Sjöstrand, *Phys. Lett.* **B351** (1995) 293.
- [2] G. Gustafson, U. Petterson and P.M. Zerwas, *Phys. Lett.* **B209** (1988) 90;  
T. Sjöstrand and V.A. Khoze, *Phys. Rev. Lett.* **72** (1994) 28; *Z. Phys.* **C62** (1994) 281;  
G. Gustafson and J. Häkkinen, *Z. Phys.* **C64** (1994) 659;  
V.A. Khoze, W.J. Stirling, S. Moretti, A. Ballestrero and E. Maina, *Z. Phys.* **C74** (1997) 493;  
A. Donnachie and P.V. Landshoff, *Phys. Lett.* **B421** (1998) 341.
- [3] S. Moretti, L. Lönnblad and T. Sjöstrand, *JHEP* **08** (1998) 001.
- [4] G. Marchesini, B.R. Webber, G. Abbiendi, I.G. Knowles, M.H. Seymour and L. Stanco, *Comp. Phys. Comm.* **67** (1992) 465.
- [5] T. Sjöstrand, *Comp. Phys. Comm.* **39** (1984) 347;  
M. Bengtsson and T. Sjöstrand, *Comp. Phys. Comm.* **43** (1987) 367.
- [6] L. Lönnblad, *Comp. Phys. Comm.* **71** (1992) 15.
- [7] ALEPH Collaboration, *Z. Phys.* **C76** (1997) 1.
- [8] S. Moretti and W.J. Stirling, *Eur. Phys. J.* **C9** (1999) 81.
- [9] N. Brown, *Z. Phys.* **C51** (1991) 107.
- [10] E. Accomando, A. Ballestrero and E. Maina, *Phys. Lett.* **B362** (1995) 141;  
M. Smith, *Eur. Phys. J.* **C9** (1999) 95.
- [11] E. Maina and M. Pizzio, *Phys. Lett.* **B369** (1996) 341.
- [12] S. Moretti, *Z. Phys.* **C75** (1997) 465; *Eur. Phys. J.* **C9** (1999) 229.
- [13] ALEPH Collaboration, *Eur. Phys. J.* **C2** (1998) 581.
- [14] For an incomplete list, see, e.g.:  
G.R. Farrar and P. Fayet, *Phys. Lett.* **B76** (1978) 575;  
T. Goldman, *Phys. Lett.* **B78** (1978) 110;  
I. Antoniadis, C. Kounnas and R. Lacaze, *Nucl. Phys.* **B211** (1983) 216;  
M.J. Eides and M.J. Vytovsky, *Phys. Lett.* **B124** (1983) 83;  
E. Franco, *Phys. Lett.* **B124** (1983) 271;  
G.R. Farrar, *Phys. Rev. Lett.* **53** (1984) 1029;  
S. Dawson, E. Eichten and C. Quigg, *Phys. Rev.* **D31** (1985) 1581;  
J. Ellis and H. Kowalski, *Phys. Lett.* **B157** (1985) 437;

- V. Barger, S. Jacobs, J. Woodside and K. Hagiwara, *Phys. Rev.* **D33** (1986) 57;  
 I. Antoniadis, J. Ellis and D.V. Nanopoulos, *Phys. Lett.* **B262** (1985) 109;  
 G.R. Farrar, *Phys. Lett.* **B265** (1991) 395;  
 M. Jezabek and J.H. Kühn, *Phys. Lett.* **B301** (1993) 121;  
 J. Ellis, D. Nanopoulos, and D. Ross, *Phys. Lett.* **B305** (1993) 375.
- [15] P. Nelson and P. Osland, *Phys. Lett.* **B115** (1982) 407;  
 B.A. Campbell, J. Ellis and S. Rudaz, *Nucl. Phys.* **B198** (1982) 1;  
 G.L. Kane and W.B. Rolnick, *Nucl. Phys.* **B217** (1983) 117;  
 B.A. Campbell, J.A. Scott and M.K. Sundaresan, *Phys. Lett.* **B126** (1983) 376.
- [16] G.R. Farrar, talk given at the ‘XIth Les Rencontres de Physique de la Vallee d’Aoste: Results and Perspectives in Particle Physics’, La Thuile, Italy, 2-8 March 1997, preprint RU-97-22, July 1997, [hep-ph/9707467](#).
- [17] L. Clavelli, P.W. Coulter and L.R. Surguladze, *Phys. Rev.* **D55** (1997) 4268;  
 L. Clavelli and L.R. Surguladze, *Phys. Rev. Lett.* **78** (1997) 1632.
- [18] F. Csikor and Z. Fodor, *Phys. Rev. Lett.* **78** (1997) 4335; talk given at the ‘International Europhysics Conference on High-Energy Physics (HEP 97)’, Jerusalem, Israel, 19-26 August 1997, preprint ITP-Budapest 538, KEK-TH-551, December 1997, [hep-ph/9712269](#).
- [19] G.R. Farrar, *Phys. Rev.* **D51** (1995) 3904; *Phys. Rev. Lett.* **76** (1996) 4111.
- [20] L. Clavelli, preprint UA-HEP-99-4, August 1999, [hep-ph/9908342](#).
- [21] G.R. Farrar, talk given at the ‘Vth International Conference on Supersymmetries in Physics (SUSY 97)’, Philadelphia, PA, 27-31 May 1997, *Nucl. Phys. Proc. Suppl.* **62** (1998) 485 (and references therein).
- [22] S. Moretti, R. Muñoz-Tapia and K. Odagiri, *Phys. Lett.* **B389** (1996) 545; *Eur. Phys. J.* **C4** (1998) 351;  
 S. Moretti, R. Muñoz-Tapia and J.B. Tausk, contribution to the XXVIIIth International Conference on High Energy Physics, Warsaw, Poland, 25-31 July 1996, preprint Cavendish-HEP-96/8, DFTT 46/96, UGR-FT-66, MZ-THEP-96-29, June 1996.
- [23] Z. Nagy and Z. Trócsányi, *Phys. Rev.* **D57** (1998) 5793.
- [24] S. Moretti and W.J. Stirling, *Phys. Lett.* **B347** (1995) 291; Erratum, *ibidem* **B366** (1996) 451.
- [25] S. Moretti, *Phys. Lett.* **B420** (1998) 367; *Nucl. Phys.* **B544** (1999) 289.
- [26] A. Ballestrero, E. Maina and S. Moretti, *Phys. Lett.* **B294** (1992) 425; *Nucl. Phys.* **B415** (1994) 265.
- [27] H. Murayama, I. Watanabe and K. Hagiwara, HELAS: HELicity Amplitude Subroutines for Feynman Diagram Evaluations, *KEK Report* 91-11, January 1992.

- [28] M. Carena, J.R. Espinosa, M. Quiros and C.E.M. Wagner, *Phys. Lett.* **B335** (1995) 209; M. Carena, M. Quiros and C.E.M. Wagner, *Nucl. Phys.* **B461** (1996) 407; H.E. Haber, R. Hempfling and A.H. Hoang, *Z. Phys.* **C75** (1997) 539.
- [29] K. Hagiwara and D. Zeppenfeld, *Nucl. Phys.* **B274** (1986) 1.
- [30] R. Kleiss and W.J. Stirling, *Nucl. Phys.* **B262** (1985) 235.
- [31] C. Mana and M. Martinez, *Nucl. Phys.* **B287** (1987) 601.
- [32] S. Moretti, *Phys. Rev.* **D50** (1994) 2016.
- [33] G.P. Lepage, *Jour. Comp. Phys.* **27** (1978) 192.
- [34] R. Kleiss, W.J. Stirling and S.D. Ellis, *Comput. Phys. Commun.* **40** (1986) 359.
- [35] Yu.L. Dokshitzer, contribution cited in the ‘Report of the Hard QCD Working Group’, Proceedings of the Workshop on ‘Jet Studies at LEP and HERA’, Durham, UK, December 1990, *J. Phys.* **G17** (1991) 1537.
- [36] A. Signer and L. Dixon, *Phys. Rev. Lett.* **D78** (1997) 811; *Phys. Rev.* **D56** (1997) 4031; A Signer, *Comp. Phys. Comm.* **106** (1997) 25; Z. Nagy and Z. Trócsányi, *Phys. Rev. Lett.* **79** (1997) 3604; *Phys. Rev.* **D59** (1999) 014020; *Phys. Rev.* **D57** (1998) 5793; J.M. Campbell, M.A. Cullen and E.W.N. Glover, *Eur. Phys. J.* **C9** (1999) 245.
- [37] F. James and M. Roos, *Comp. Phys. Comm.* **10** (1975) 343.
- [38] S. Moretti and J.B. Tausk, *Z. Phys.* **C69** (1996) 635.
- [39] L. Clavelli and G.v. Gehlen, *Phys. Rev.* **D27** (1983) 1495.
- [40] A. Ballestrero, E. Maina and S. Moretti, *Phys. Lett.* **B333** (1994) 434.
- [41] See, e.g.:  
A. Djouadi, D. Haidt, B.A. Kniehl, B. Mele and P.M. Zerwas, in Proceedings of the Workshop ‘ $e^+e^-$  Collisions at 500 GeV. The Physics Potential’, Munich, Annecy, Hamburg, 3–4 February 1991, ed. P.M. Zerwas, DESY 92-123A, August 1992, page 11;  
A. Djouadi, J. Kalinowski and P.M. Zerwas, *ibidem*, page 83.

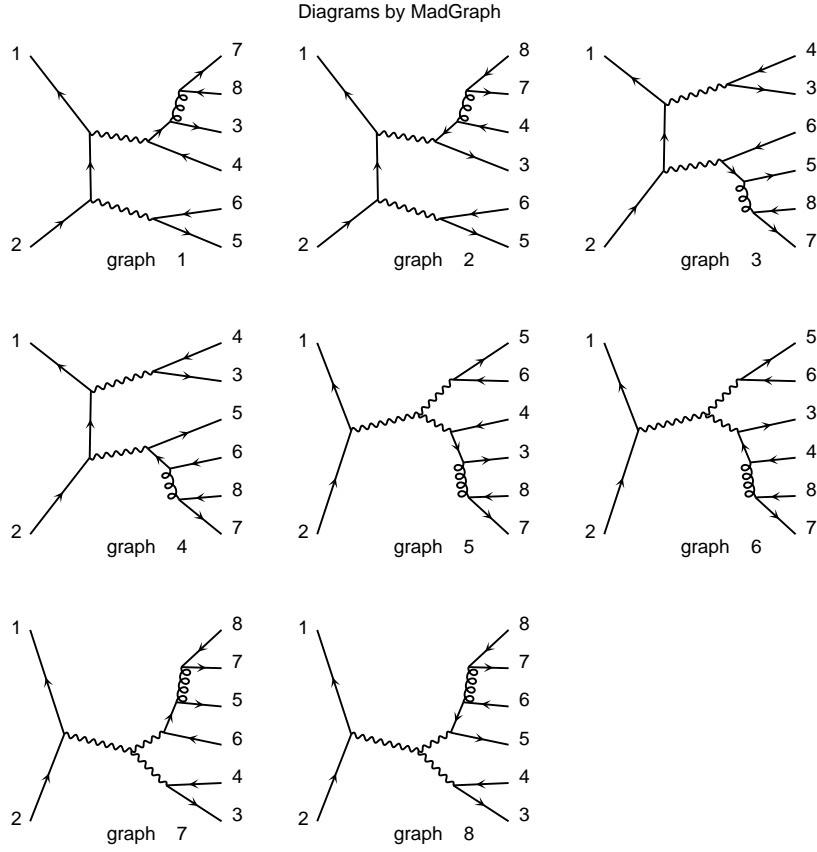


Figure 1: Feynman diagrams contributing to  $e^+(1) + e^-(2) \rightarrow q(3) + \bar{q}(4) + q'(5) + \bar{q}'(6) + q''(7) + \bar{q}''(8)$ , via  $W^+W^-$  production and decay, through the order  $\mathcal{O}(\alpha_{em}^4 \alpha_s^2)$ . Here, we assume  $q'' \neq q', q$ . An internal wavy line represents a  $\gamma, Z$  or a  $W^\pm$ , as appropriate.

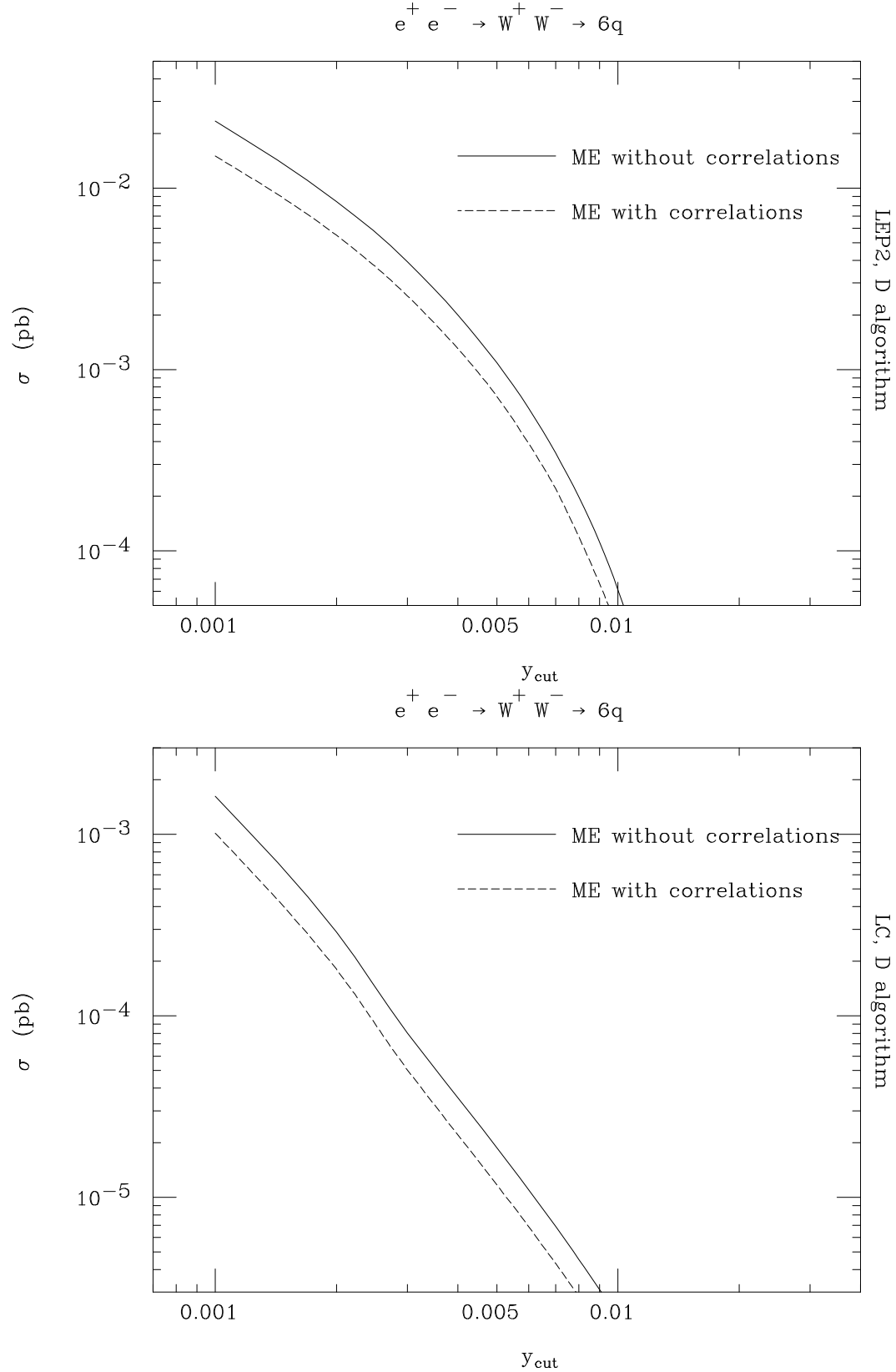


Figure 2: Cross section for  $e^+e^- \rightarrow W^+W^- \rightarrow q\bar{q}q'\bar{q}'q''\bar{q}''$  events as a function of the resolution parameter  $y_{\text{cut}}$  in the Durham jet-finder, at  $E_{\text{cm}} = 172$  (above) and 350 (below) GeV. The summation over all possible combinations of flavours  $q$ ,  $q'$  and  $q''$  has been performed. Solid: without Fermi-Dirac correlations. Dashed: with Fermi-Dirac correlations.

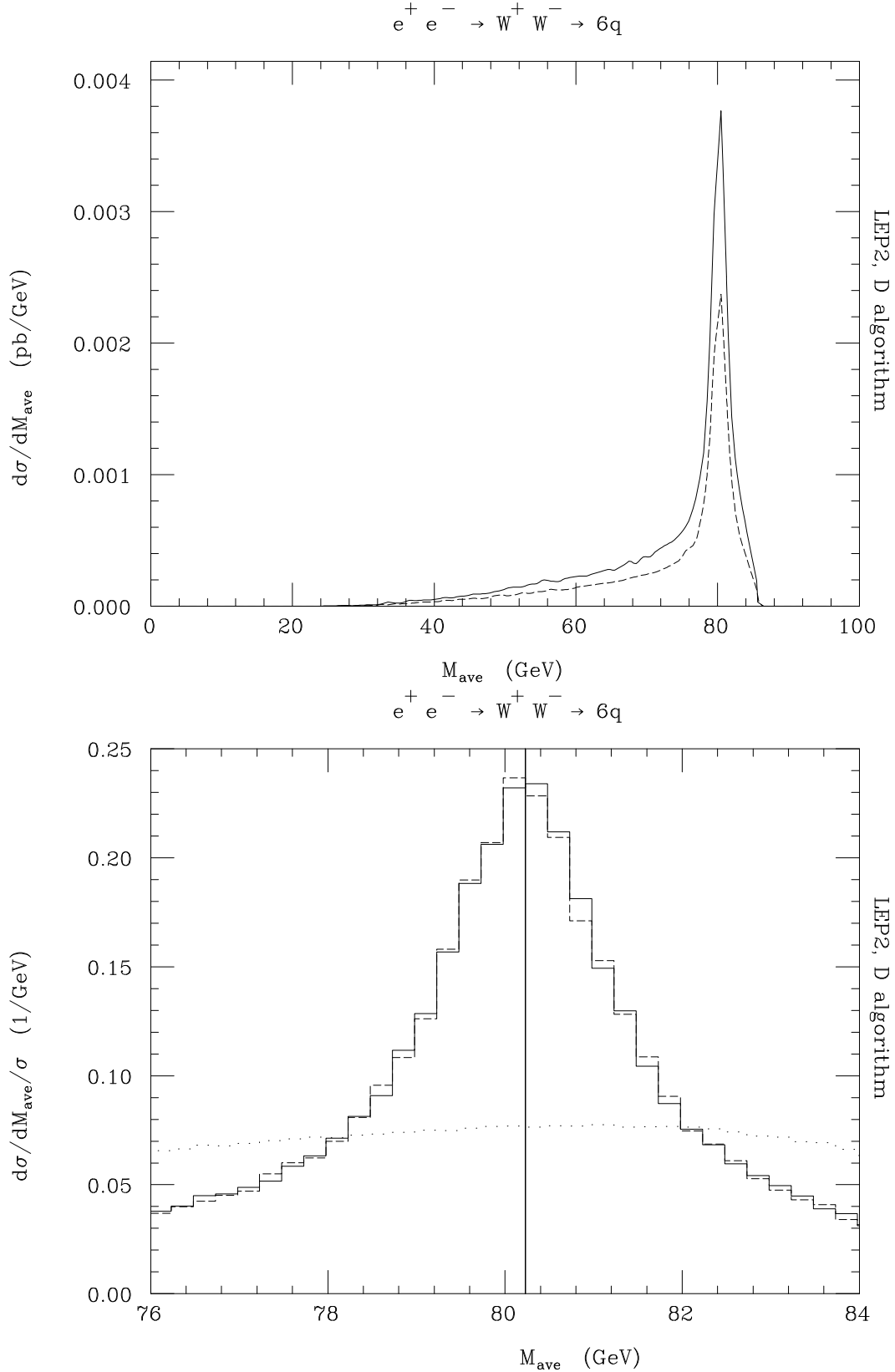


Figure 3: Differential distributions in the ‘average value’ of the best reconstructed  $W^\pm$  masses for  $e^+e^- \rightarrow W^+W^- \rightarrow q\bar{q}q'\bar{q}'q''\bar{q}''$  events (solid and dashed lines) and a for pure phase-space model of six-particle production (dotted line, below only), with  $y_{\text{cut}} = 0.001$  in the Durham jet-finder, at  $E_{\text{cm}} = 172$  GeV. The summation over all possible combinations of flavours  $q, q'$  and  $q''$  has been performed. Solid with  $\times$ : Epi-Dip production. Dashed with  $\times$ : Epi-Dip

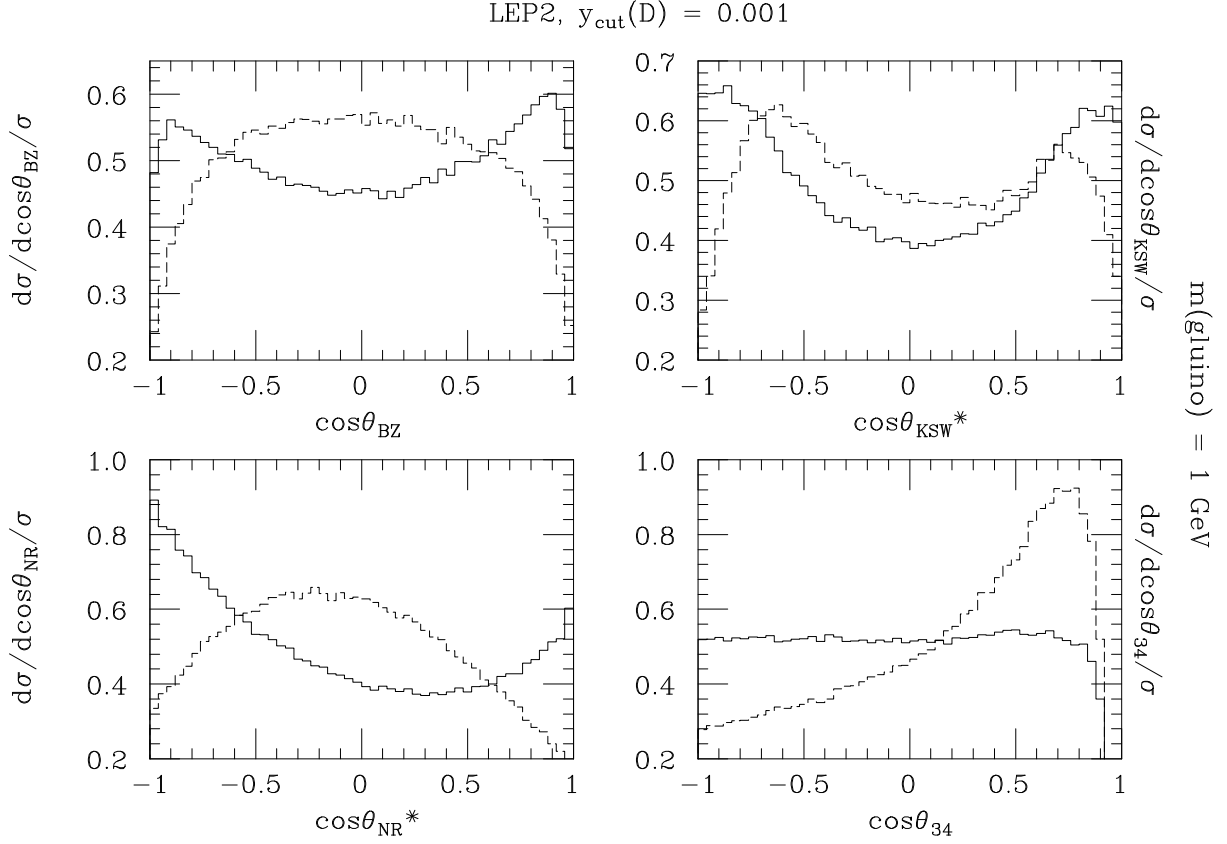


Figure 4: Differential distributions in the cosine of the following angular variables: (top-left)  $\chi_{\text{BZ}}$ , (top-right)  $\Phi_{\text{KSW}}^*$ , (bottom-left)  $\theta_{\text{NR}}^*$  and (bottom-right)  $\theta_{34}$ , for  $e^+e^- \rightarrow W^+W^- \rightarrow q\bar{q}q'\bar{q}'gg$  (solid lines) and  $e^+e^- \rightarrow W^+W^- \rightarrow q\bar{q}q'\bar{q}'\tilde{g}\tilde{g}$  (dashed lines) events, for  $m_{\tilde{g}} = 1 \text{ GeV}$ , with  $y_{\text{cut}} = 0.001$  in the Durham jet-finder, at  $E_{\text{cm}} = 172 \text{ GeV}$ . The summation over all possible combinations of flavours  $q$  and  $q'$  has been performed. Spectra are normalised to unity.

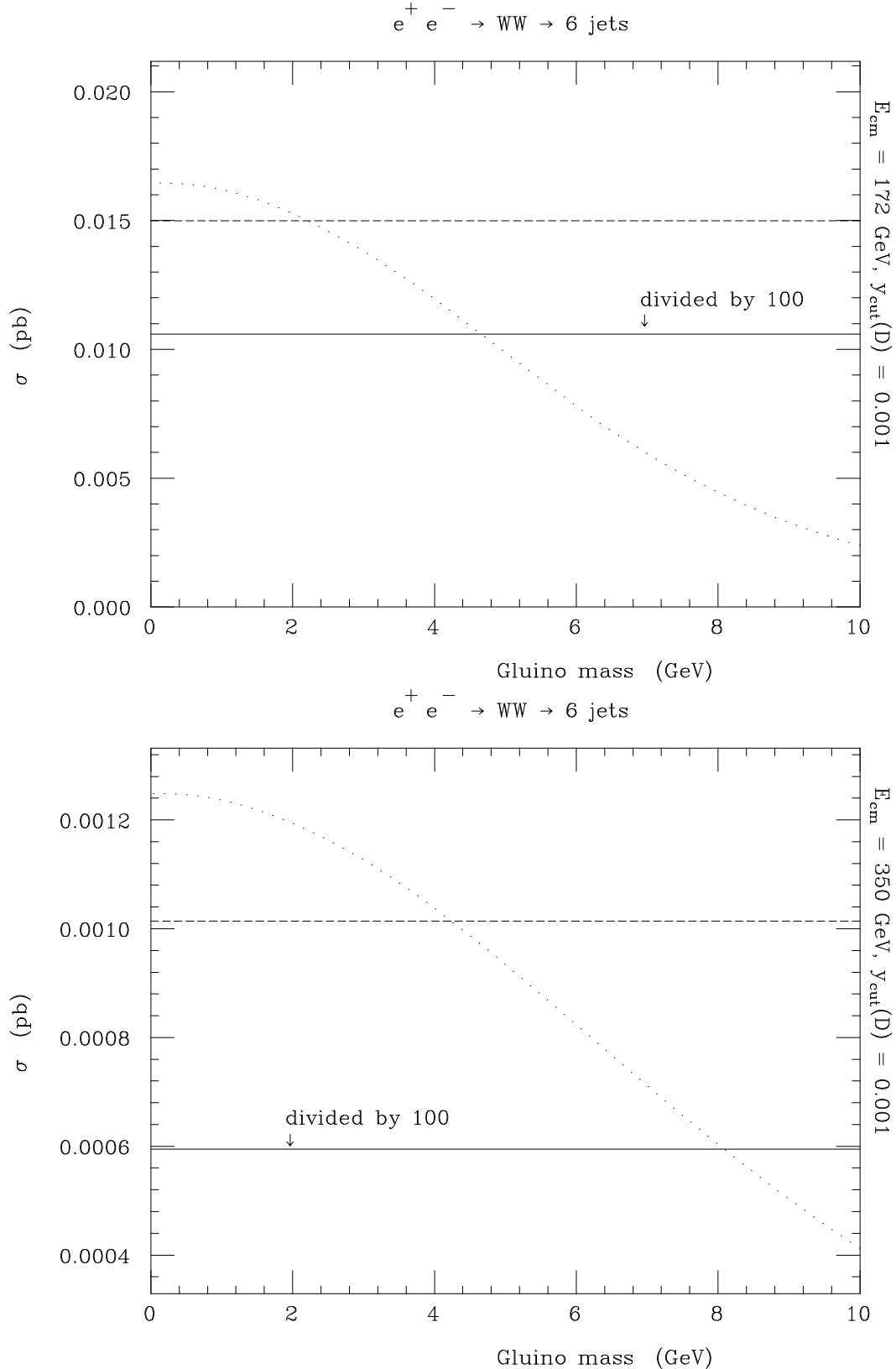


Figure 5: Cross section for  $e^+e^- \rightarrow W^+W^- \rightarrow q\bar{q}q'\bar{q}'gg$  (solid lines),  $e^+e^- \rightarrow W^+W^- \rightarrow q\bar{q}q'\bar{q}'q''\bar{q}''$  (dashed lines) and  $e^+e^- \rightarrow W^+W^- \rightarrow q\bar{q}q'\bar{q}'\tilde{g}\tilde{g}$  (dotted lines) events as a function of the gluino mass, with  $y_{\text{cut}} = 0.001$  in the Durham jet-finder, at  $E_{\text{cm}} = 172$  (upper plot) and 350 GeV (lower plot). The summation over all possible combinations of flavours  $q$  and  $q'$  has been performed. Six-quark rates include Fermi-Dirac correlations. Gluon rates have been divided by

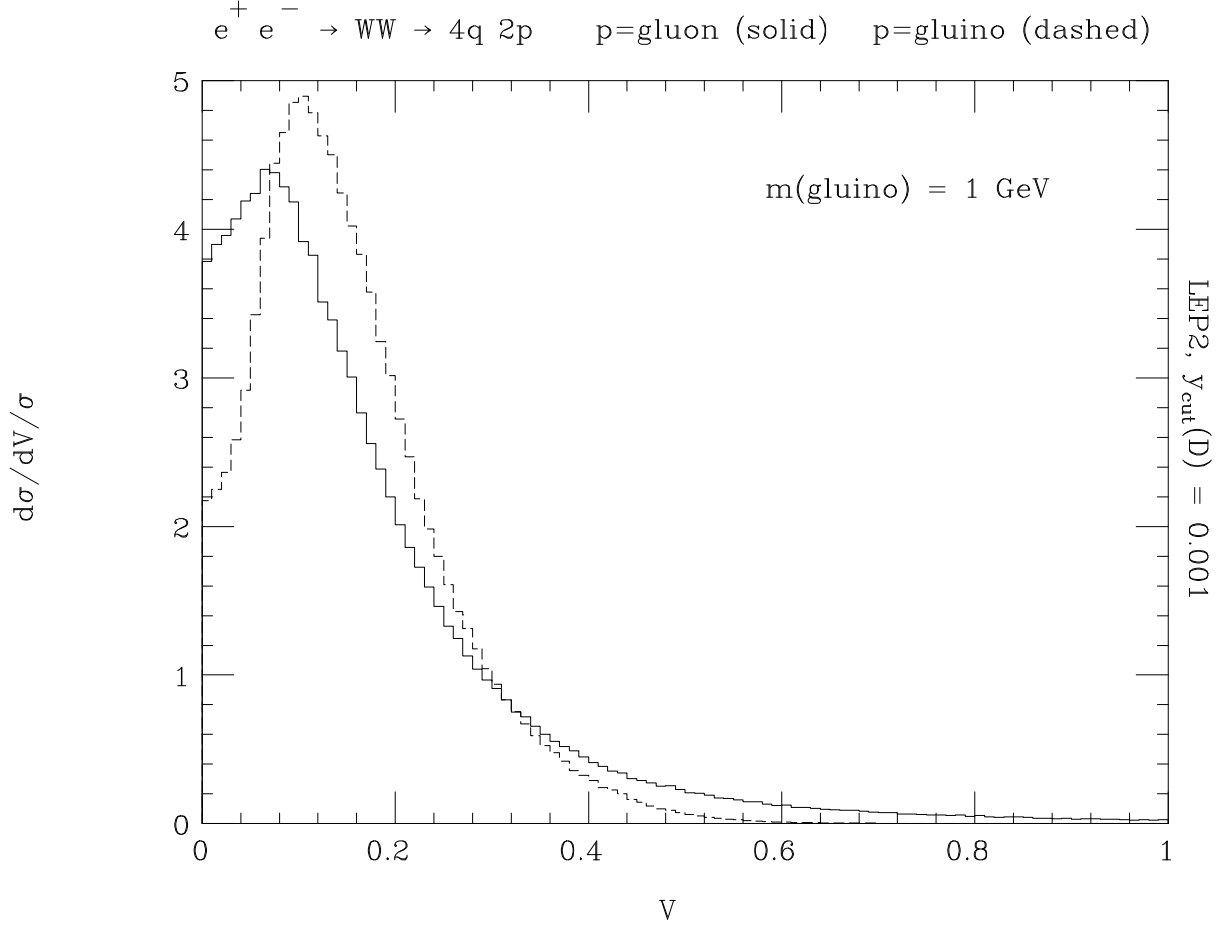


Figure 6: Differential distributions in the quantity defined in eq. (31) of the resonant four-jet subsystem for  $e^+e^- \rightarrow W^+W^- \rightarrow q\bar{q}q'\bar{q}'gg$  (solid lines) and  $e^+e^- \rightarrow W^+W^- \rightarrow q\bar{q}q'\bar{q}'\tilde{g}\tilde{g}$  (dashed lines) events, for  $m_{\tilde{g}} = 1 \text{ GeV}$ , with  $y_{\text{cut}} = 0.001$  in the Durham jet-finder, at  $E_{\text{cm}} = 172 \text{ GeV}$ . The summation over all possible combinations of flavours  $q$  and  $q'$  has been performed. Spectra are normalised to unity.

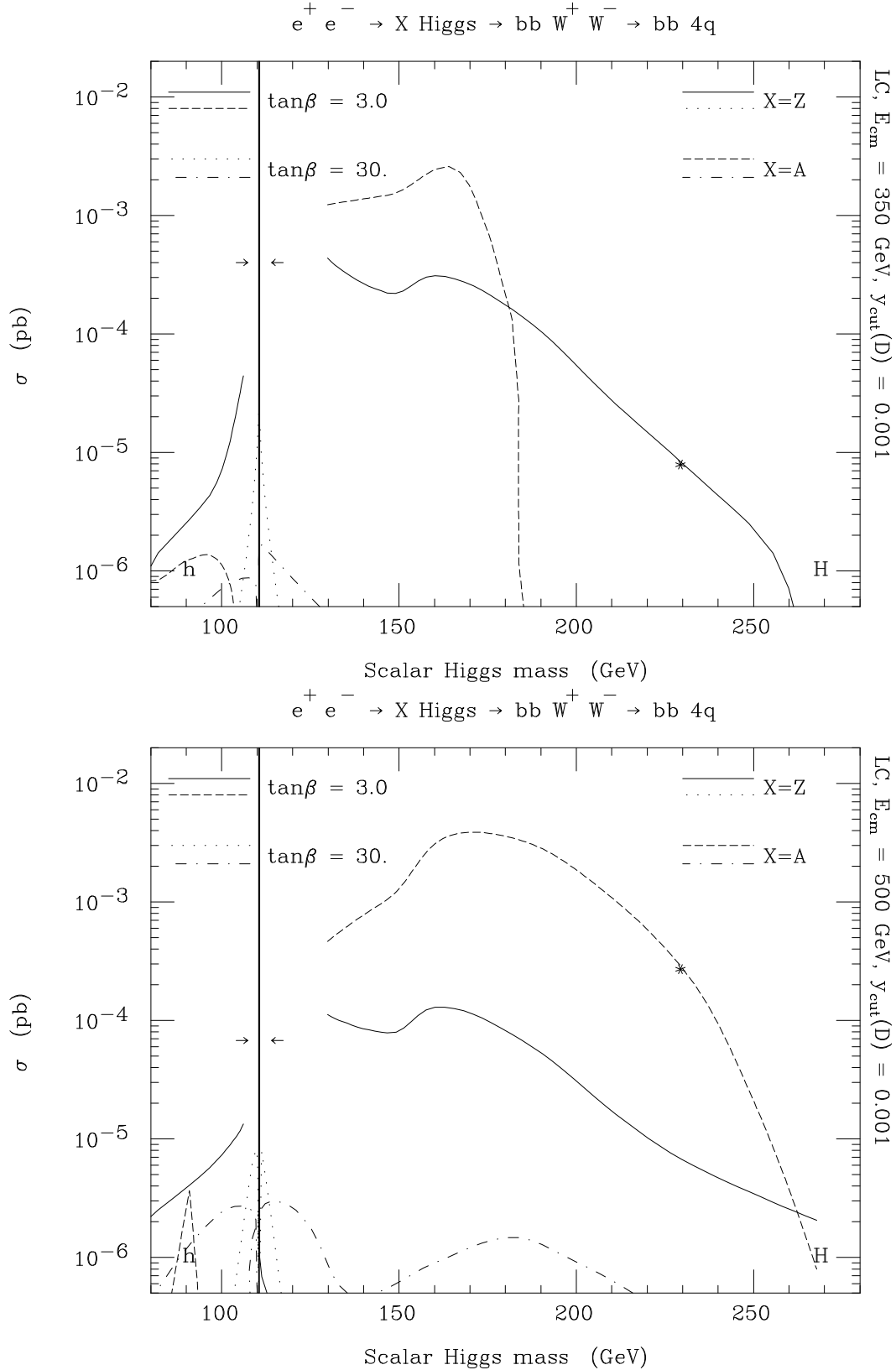


Figure 7: Cross section for  $e^+e^- \rightarrow \Phi Z \rightarrow W^+W^-Z \rightarrow q\bar{q}q'\bar{q}'b\bar{b}$ ,  $e^+e^- \rightarrow \Phi A \rightarrow W^+W^-A \rightarrow q\bar{q}q'\bar{q}'b\bar{b}$  (solid, dashed, dotted and dot-dashed lines) and  $e^+e^- \rightarrow W^+W^- \rightarrow q\bar{q}q'\bar{q}'b\bar{b}$  (arrows) events as a function of the scalar Higgs masses  $M_h$  and  $M_H$ , with  $y_{\text{cut}} = 0.001$  in the Durham jet-finder, at  $E_{\text{cm}} = 350$  (upper plot) and  $500$  (lower plot) GeV. The summation over all possible combinations of flavours  $q$  and  $q'$  has been performed

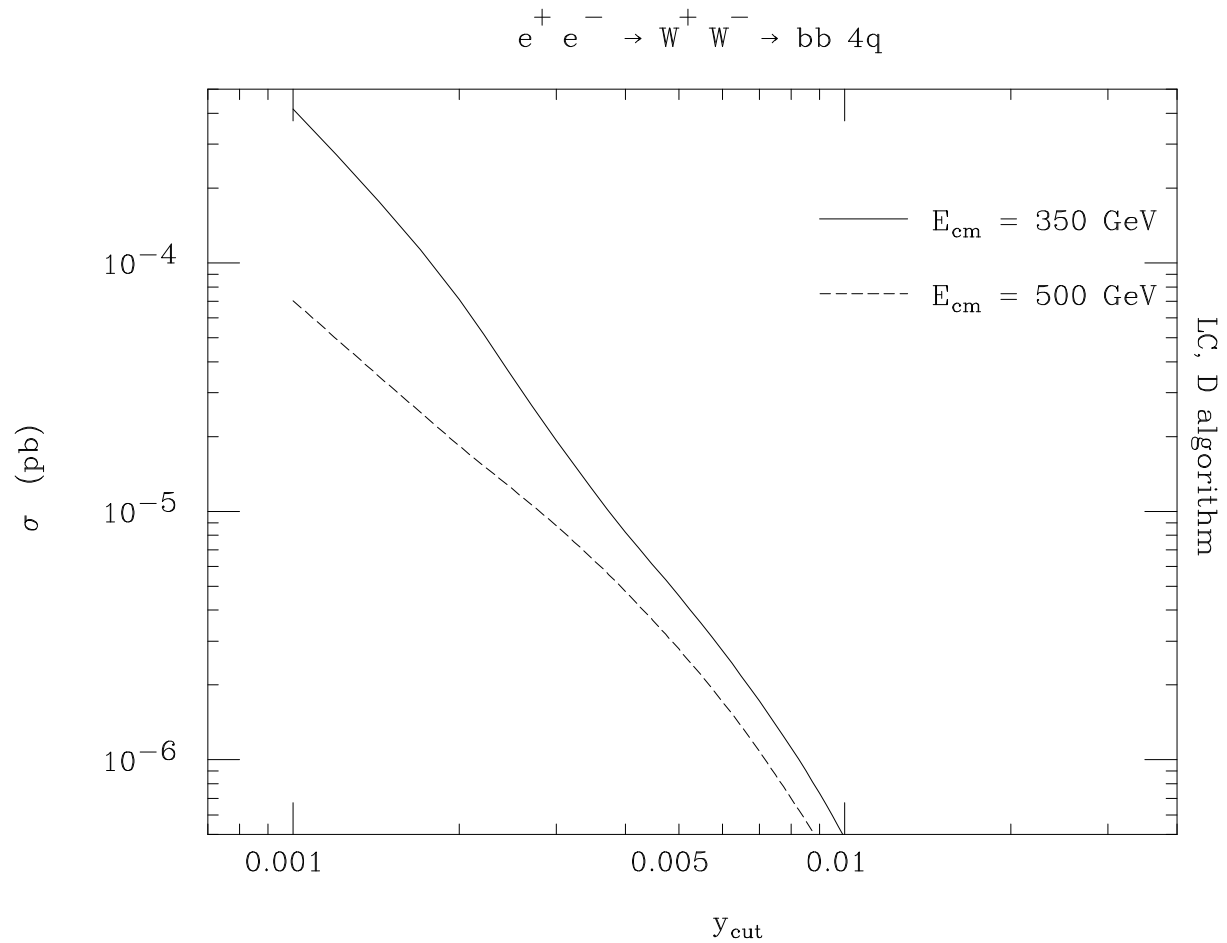


Figure 8: Cross section for  $e^+e^- \rightarrow W^+W^- \rightarrow q\bar{q}q'\bar{q}'b\bar{b}$  events as a function of the resolution parameter  $y_{\text{cut}}$  in the Durham jet-finder, at  $E_{\text{cm}} = 350$  (solid line) and 500 (dashed line) GeV. The summation over all possible combinations of flavours  $q$  and  $q'$  has been performed.

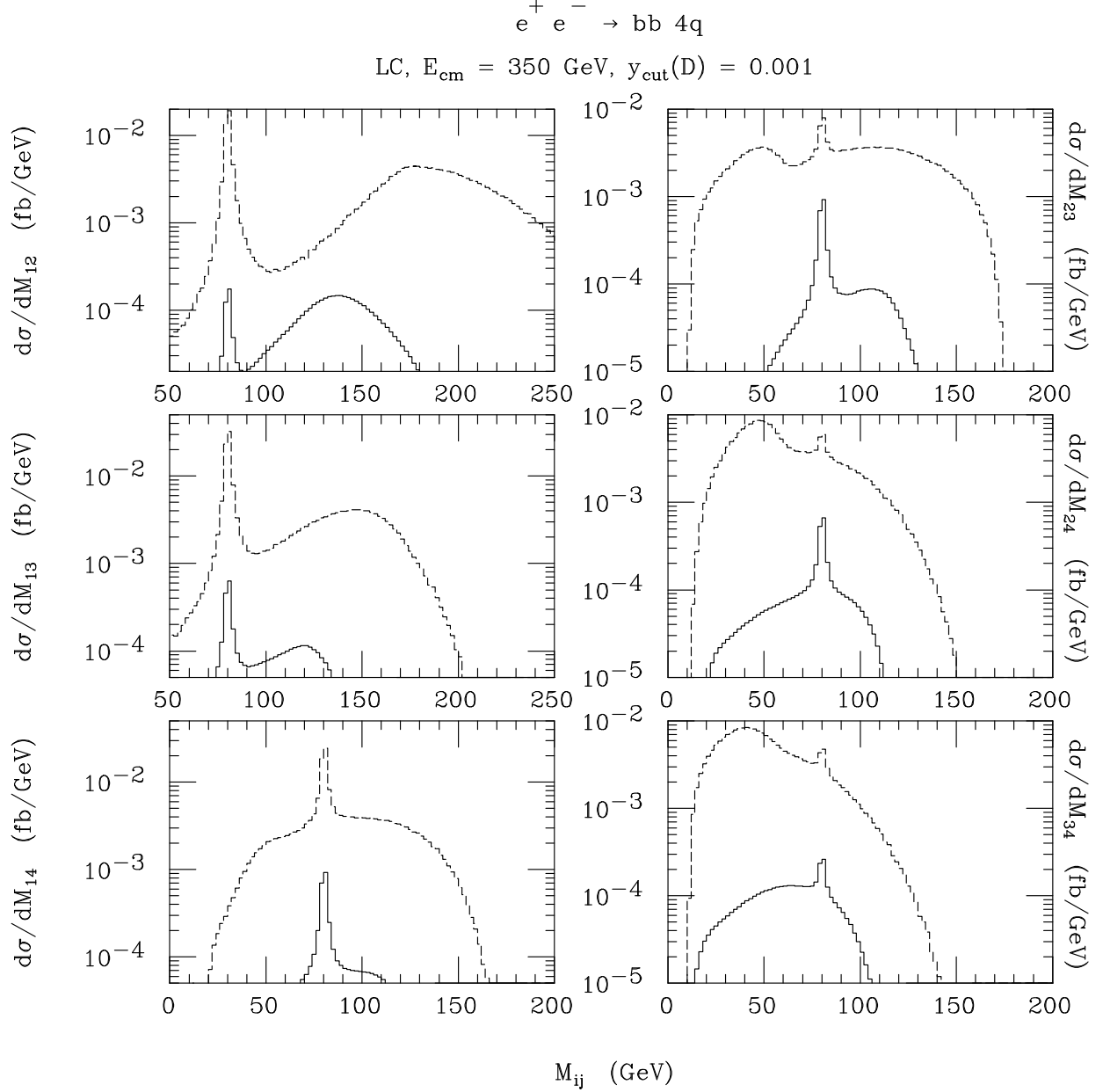


Figure 9: Differential distributions in the invariant mass of the energy-ordered di-jet pairs,  $M_{ij}$  with  $i < j = 1, \dots, 4$ , for  $e^+e^- \rightarrow HZ \rightarrow W^+W^-Z \rightarrow q\bar{q}q'\bar{q}'b\bar{b}$  (solid lines) and  $e^+e^- \rightarrow W^+W^- \rightarrow q\bar{q}q'\bar{q}'b\bar{b}$  (dashed lines) events, in the MSSM for  $M_A = 220\text{ GeV}$  and  $\tan\beta = 3.0$ , with  $y_{\text{cut}} = 0.001$  in the Durham jet-finder, at  $E_{\text{cm}} = 350\text{ GeV}$ . The summation over all possible combinations of flavours  $q$  and  $q'$  has been performed. Spectra are normalised to the total cross sections.

$$e^+ e^- \rightarrow bb \ 4q$$

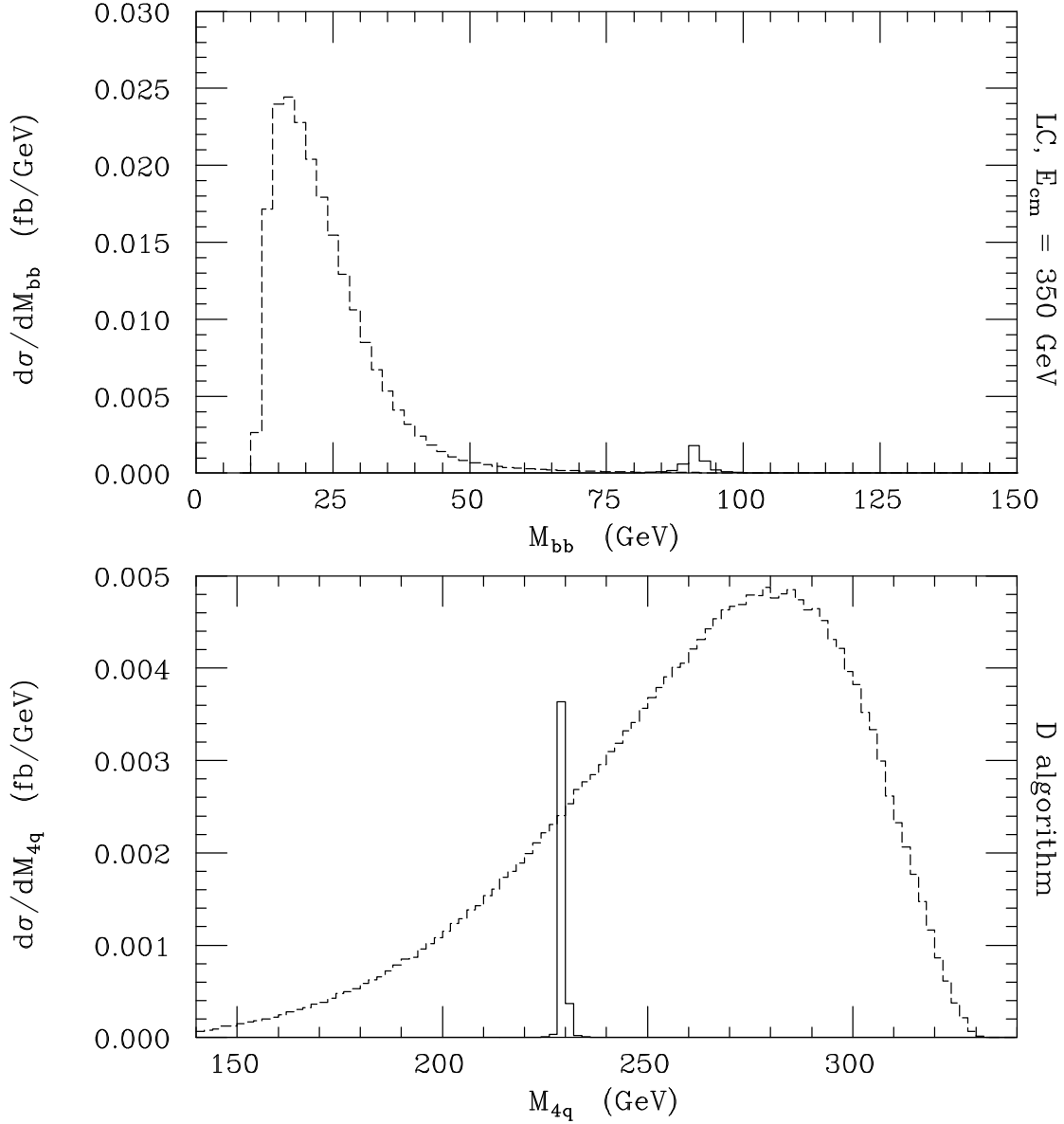


Figure 10: Differential distributions in the invariant mass of the  $b\bar{b}$ ,  $M_{b\bar{b}}$  (upper plot), and four-light-quark,  $M_{4q}$  (lower plot), systems, for  $e^+e^- \rightarrow HZ \rightarrow W^+W^-Z \rightarrow qq'q'\bar{q}\bar{q}$  (solid lines) and  $e^+e^- \rightarrow W^+W^- \rightarrow qq'q'\bar{q}\bar{q}$  (dashed lines) events, in the MSSM for  $M_A = 220 \text{ GeV}$  and  $\tan\beta = 3.0$ , with  $y_{\text{cut}} = 0.001$  in the Durham jet-finder, at  $E_{\text{cm}} = 350 \text{ GeV}$ . The summation over all possible combinations of flavours  $q$  and  $q'$  has been performed. Spectra are normalised to the total cross sections.

$$e^+ e^- \rightarrow bb 4q$$

LC,  $E_{\text{cm}} = 350 \text{ GeV}$ ,  $y_{\text{cut}}(\text{D}) = 0.001$

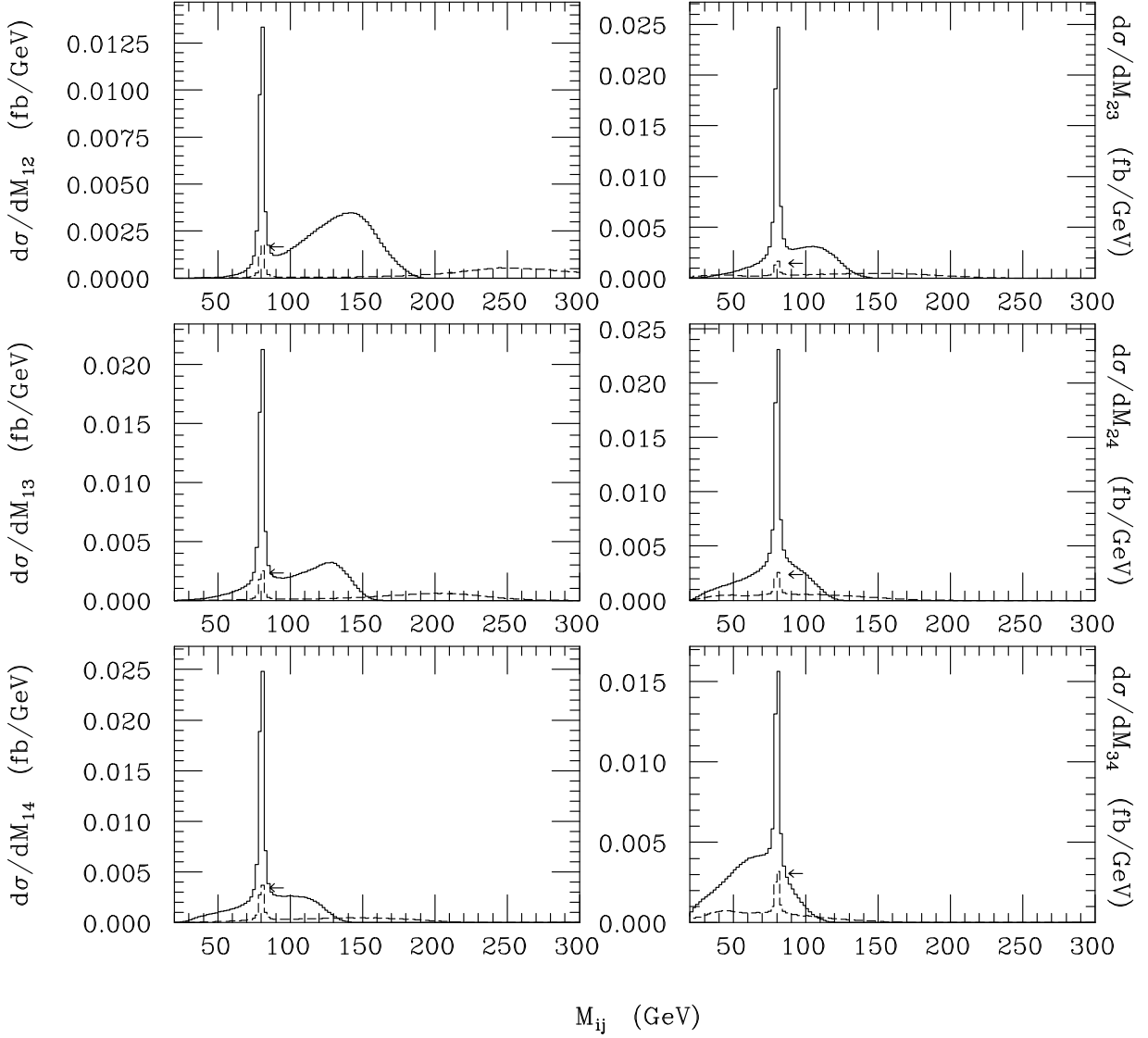


Figure 11: Differential distributions in the invariant mass of the energy-ordered di-jet pairs,  $M_{ij}$  with  $i < j = 1, \dots, 4$ , for  $e^+e^- \rightarrow HA \rightarrow W^+W^-A \rightarrow q\bar{q}q'\bar{q}'b\bar{b}$  (solid lines) and  $e^+e^- \rightarrow W^+W^- \rightarrow q\bar{q}q'\bar{q}'b\bar{b}$  (dashed lines, where the peak height is denoted by an arrow) events, in the MSSM for  $M_A = 220 \text{ GeV}$  and  $\tan\beta = 3.0$ , with  $y_{\text{cut}} = 0.001$  in the Durham jet-finder, at  $E_{\text{cm}} = 500 \text{ GeV}$ . The summation over all possible combinations of flavours  $q$  and  $q'$  has been performed. Spectra are normalised to the total cross sections.

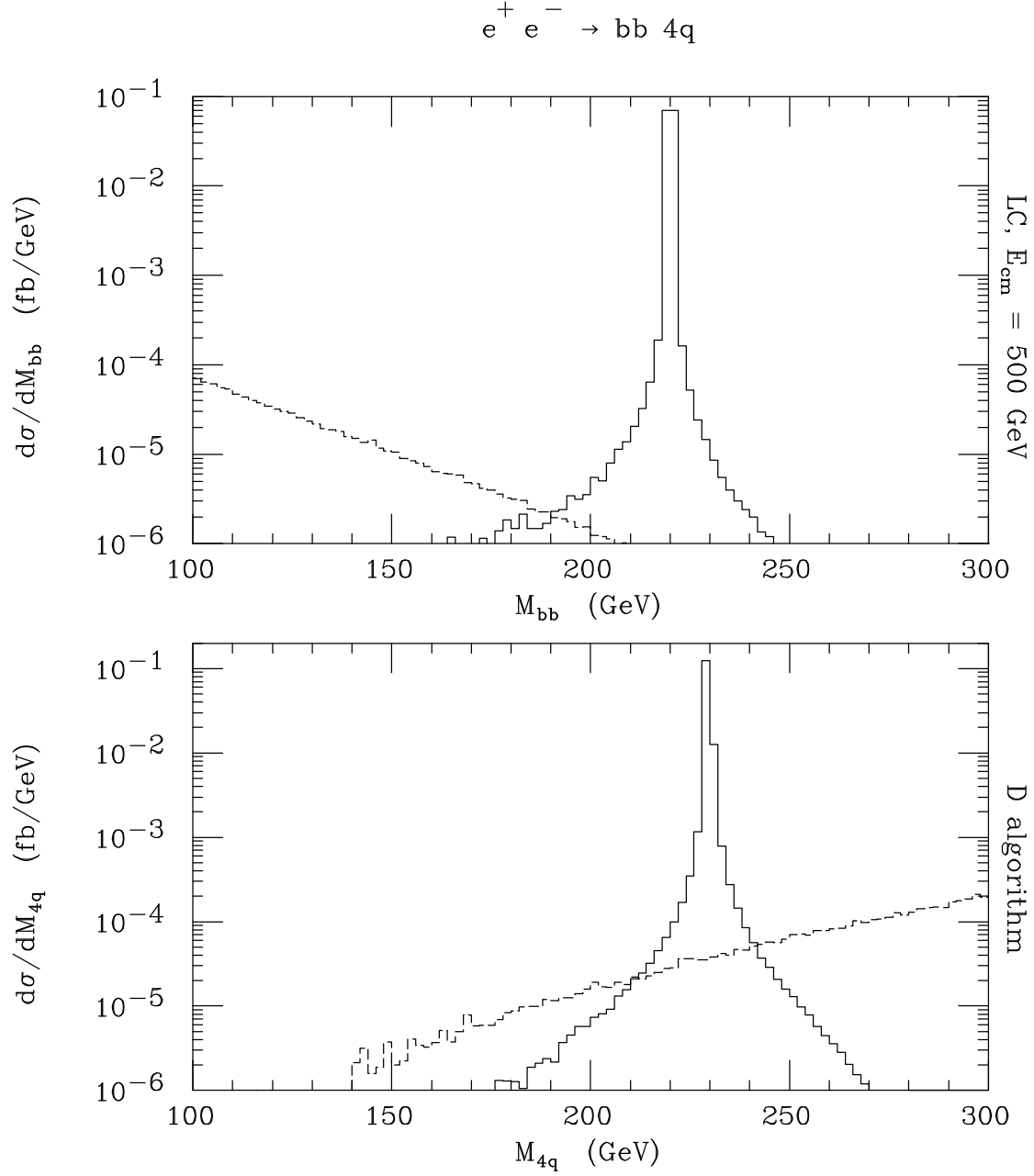


Figure 12: Differential distributions in the invariant mass of the  $b\bar{b}$ ,  $M_{b\bar{b}}$  (upper plot), and four-light-quark,  $M_{4q}$  (lower plot), systems, for  $e^+e^- \rightarrow HA \rightarrow W^+W^-A \rightarrow qq'q'\bar{q}\bar{b}\bar{b}$  (solid lines) and  $e^+e^- \rightarrow W^+W^- \rightarrow qq'q'\bar{q}\bar{b}\bar{b}$  (dashed lines) events, in the MSSM for  $M_A = 220$  GeV and  $\tan\beta = 3.0$ , with  $y_{\text{cut}} = 0.001$  in the Durham jet-finder, at  $E_{\text{cm}} = 500$  GeV. The summation over all possible combinations of flavours  $q$  and  $q'$  has been performed. Spectra are normalised to the total cross sections.